Letter to Editor,

Prof. Martin Heimann

Dear Prof Martin Heimann, 25 June 2018

We have now completed our responses to the Referees' comments and revised our manuscript:

Unprecedented strength of Hadley circulation in 2015-2016 impacts on CO_2 interhemispheric difference, by J. S. Frederiksen and R. J. Francey

for submission for journal publication in Atmospheric Chemistry and Physics.

We believe that we have satisfactorily answered and responded to all the three referees' questions and suggestions. In particular:

1. We have responded in detail to the points made by RC1 including expanding the study to examine the role of interannual changes in mean and eddy transports, as characterized by our dynamical indices, on five other trace gas species namely CH_4, CO, H_2, N_2O and SF_6 .
2. We have also confirmed the robustness of our conclusions based on NCEP-NCAR data by redoing the main calculations with dynamical indices based on NASA MERRA atmospheric circulation data as suggested by RC2.
3. We have provided a more in-depth discussion of the role of surface fluxes as well as transport in the interannual variability of CO_2 interhemispheric gradient as suggested by the three Referees.
4. We now discuss how the location of the warm water varies for the 1997-1998, 2009-2010 and 2015-2016 El Niños and the likely causes of the differences in CO_2 interhemispheric gradient, as suggested by RC3.
5. We now also discuss the Atlantic duct, the Walker circulation, Rossby wave breaking and make the paper more self contained in the Supplement as suggested by the three Referees.

We have responded to the comments of the three Referees in the form needed by ACP: (1) comments from Referees, (2) author's response, (3) author's changes to manuscript. Our three responses detail the changes that we have made to the manuscript for submission for journal publication in ACP. Briefly, we have included the role of mean and eddy transport on interhemispheric gradients of other trace gases as a new Section 6. Additional information on atmospheric circulation and Rossby waves are contained in the Supplement.

Yours sincerely,

Jorgen Frederiksen and Roger Francey

Unprecedented strength of Hadley circulation in 2015-2016 impacts on CO_2 interhemispheric difference

Jorgen S. Frederiksen and Roger J. Francey

CSIRO Oceans and Atmosphere, Aspendale, Victoria, AUSTRALIA

Correspondence to: Jorgen S. Frederiksen (jorgen.frederiksen@csiro.au)

Response Part 2 to Anonymous Referee 1 (RC1) review:

As noted in our first Response to RC1: "We thank the Referee for the thoughtful comments which have led us to examine a large number of other trace gases and their relationships to our dynamical indices. We have carried out extra seasonal correlations between the Mauna Loa minus Cape Grim difference in trace gas species (CH_4, CO, H_2, N_2O) routinely monitored by CSIRO with the our dynamical indices. We have also included corresponding correlations using NOAA SF_6 data. In each case we have briefly examined biogeochemical factors that influence differences in inter-hemispheric fluxes from one species to the next. We believe that our findings detailed in the associated Supplement provide very strong evidence of the relationships between the Mauna Loa minus Cape Grim difference in trace gases (CO_2 presented in the main paper) and dynamical indices of eddy and mean transport."

We have now restructured our manuscript and included the discussion of the other trace gases in the main paper. We have also added Section 2.1 where the role of surface fluxes is discussed in more detail. We summarize here these additional changes. The new Supplement still contains detailed evidence of the role of topographic Rossby waves during the 17 February 2015 episode of wave trains seen in the OCO-2 data and some extra material on the westerly ducts had been added.

Question 1

Comments from Referee:

Pg2, Lines 10-13: I have some trouble to believe this interpretation. A lot of CO2 or XCO2 variations are flux driven, and land flux is governed by weather and climate.

Author's response:

We agree with the reviewer that changes in surface fluxes can be a very important component in the interhemispheric differences in these trace gases as is now discussed in a new Subsection 2.1 on extratropical terrestrial flux variation.

Author's changes to manuscript:

2.1 The influences of terrestrial fluxes and transport on interhemispheric CO_2 differences

The growth rate and concentration of atmospheric CO_2 depend on many mechanisms including fossil fuel emissions, surface fluxes, such as associated with the growth and decay of vegetation, and atmospheric mean and eddy transport. The CO_2 growth rate and IH gradients in CO_2 vary on daily, monthly, yearly and multi-year time scales where there is a quasi-periodic variability associated with the influence of ENSO (e.g. Thoning et al. 1989). This reflects the response of tropical vegetation to rainfall variations and both hemispheres are also affected through dynamical coupling.

A number of recent inversion studies have largely attributed growth anomalies in atmospheric CO_2 concentrations to anomalous responses of the terrestrial biosphere. However, the variability in the responses within Dynamic Global Vegetation Models (DGVMs) is significant. Le Quéré et al. (2017) for example note that the "standard deviation of the annual CO_2 sink across the DGVMs averages to ± 0.8 GtC yr^{-1} for the period 1959 to 2016". This is significantly larger than the reported extratropical sink anomalies during for example the major 2009-2010 step in CO_2 concentrations (Poulter et al., 2014; Trudinger et al., 2016). Francey and Frederiksen (2015) presented reasons supporting a dynamical contribution to the cause of the 2009-2010 $C_{mlo-cgo}$ step.

For the 2015-2016 period of particular relevance here there are two studies that stand out. Keenan et al. (2016) interpret slowing CO_2 growth in 2016 as strong uptake by Northern Hemisphere terrestrial forests. Yue et al. (2018) examine the reasons for the strong positive anomalies in atmospheric CO_2 growth rates during 2015. They present evidence of the Northern Hemisphere terrestrial response to El Niño events by way of satellite observations of vegetation greenness. To reconcile increased greenness with increased CO_2 growth their inversion modelling requires the "largest ever observed" transition from sink to source in the tropical biosphere at the peak of the El Niño, "but the detailed mechanisms underlying such an extreme transition remain to be elucidated".

In this study, we find that the 2015-2016 El Niño also corresponds to unprecedented anomalies in both mean and eddy IH CO_2 transport characterized by indices of these transfers that we introduce, affecting Northern Hemisphere CO_2 growth. As for the anomalies in CO_2 IH gradient during the 2009-2010 El Niño, studied in FF16, this again suggests a contributing role for anomalous IH transport during the 2015-2016 event. We examine this possibility in detail and study the relationships between the extremes in IH CO_2 differences and transport anomalies for 1992 to 2016 and associated correlations between $C_{mlo-cgo}$ (and other trace gases) and dynamical indices of transport.

Question 2

The interactions of fluxes and transport causes these XCO2 wave trains.

Author's response:

As noted in our first Response to RC1: "We now provide in the Supplement detailed evidence of the role of topographic Rossby waves during the 17 February 2015 episode of wave trains seen in the OCO-2 data. We also discuss the role vertical uplift during that event. We consider the coincidence of timing, location, orientation and wave number of the Rossby waves observed by OCO-2 with dynamical theory as being compelling evidence for our interpretation." Additional material on the westerly ducts has also been added.

Author's changes to manuscript:

SUPPLEMENTARY INFORMATION

1 Pacific and Atlantic westerly ducts

The interhemispheric response to mid-latitude forcing produced by Rossby dispersion through equatorial westerly ducts was documented by Webster and Holton (1982). The zonal winds in the equatorial troposphere are generally easterly but in the upper troposphere the winds may be westerly in the Pacfic duct (centred on 5°N-5°S, 140°W-170°W) or the Atlantic duct (centred on 5°N-5°S, 10°W-40°W) as shown in Figure 2 of Webster and Chang (1988). As discussed in Francey and Frederiksen (2016, denoted FF16), and shown in Figure 1S for the period 1992 to 2016 of interest here, the upper-tropospheric zonal wind is strongly correlated with the SOI in the Pacific duct region and anti-correlated in the Atlantic duct region. As the atmospheric circulation changes between La Niña and El Niño conditions the warm ocean temperatures move from the western to eastern Pacific. The upward branch of the Walker circulation follows the warm water and the associated upper-tropospheric westerlies to the east of the uplift successively open the Pacific westerly duct and then the Atlantic westerly duct (Figure 1 of Webster and Chang 1988). This is the reason for the correlations in our Figure 1S. The strength (and sign) of the upper-tropospheric zonal velocity in the near-equatorial regions is correlated with corresponding levels in the turbulent kinetic energy which is generated by Rossby wave breaking (Figure 6 of Frederiksen and Webster 1988). The Pacific duct, u_{duct} of Table 1, is in general the dominant duct as shown in Figure 2S which depicts the boreal winter (Dec-Feb) upper tropospheric vector wind for 1992-2016.

2 Topographic Rossby waves during February 2015

As noted in the Introduction, the NASA (2016) OCO-2 CO_2 concentration in Figure 1(a) shows Rossby wave trains over the eastern Pacific and across South America on 17 February 2015. This episode is characteristic of other times of IH Rossby wave propagation during the boreal winter–spring, and particularly February, of 2015. The average 17 to 18 February 2015 streamfunction anomaly, from the thirty year 1981–2010 mean for the same period, is shown in Figure 3S(a) for the Western Hemisphere (0°W–180°W) between 60°S and 60°N and at the $\sigma = 0.2582$ level. Here $\sigma = \frac{pressure}{surface\ pressure}$ and the corresponding pressure level is circa 260 hPa. We note that the phase lines broadly run from SW to NE between the Southern and Northern Hemispheres but are modulated by some smaller scale features. Moreover the dominant zonal wavenumber $m = 4$.

Indeed there are broad similarities between the streamfunction anomaly in Figure 3S(a) and the streamfunction for the purely topographic Rossby waves in Figures 3a and b of Frederiksen and O'Kane (2005). For both the observations considered here and the ensemble of nonlinear simulations and statistical closure calculations the phase lines in the Western Hemisphere run SW to NE and the dominant wavenumber is 4. The dominant wavenumber 4 is also clearly seen in the energy spectra in Figure 2 of Frederiksen and O'Kane (2005). The SW to NW phase lines of pure topographic Rossby waves are also seen in the linear calculations in Figure 6 of Frederiksen (1982). In both the linear and nonlinear calculations the topographic Rossby waves are generated by the interaction of westerly winds with a conical mountain located at 30° N (an idealized representation of the massive Himalayan orography) and for a situation where the near equatorial winds are westerly. For the observational results in Figure 3S(a), the near equatorial winds between 5°S and 5°N are westerly in the Western Hemisphere broadly above 400 hPa and easterly below (not shown).

Figure 3S(b) shows the 300 hPa zonal wind anomaly corresponding to the average 17 to 18 February streamfunction anomaly in Figure 3S(a). Again the SW to NE phase lines are evident as is the dominant $m = 4$ wavenumber although the presence of smaller scale features associated with disturbances in the storm tracks (typically $m \sim 8-12$) is perhaps more evident. In Figures 4S(a) and 4S(b) we depict latitude pressure cross sections of the zonal wind anomalies for 17 to 18 February averaged between 120°W–140°W and 80°W–100°W respectively. We note that the anomaly is largely equivalent barotropic, as expected for topographic Rossby waves, and, by comparing the two panels, the SW to NW phase tilt is evident throughout the atmosphere. It can also be seen that the propagation across the equator into the Southern Hemisphere occurs primarily in the upper troposphere, particularly between 80°W–100°W where the mean westerly winds are weaker (not shown).

We have also plotted latitude pressure cross sections of anomalies of the vertical velocity in pressure coordinates, $\omega = dp/dt$ where p is pressure, for 17 to 18 February averaged between 120°W–140°W and 80°W–100°W (not shown). These cross sections indicate that there is strong uplift in the Northern Hemisphere between 10°N and 30°N (negative ω) and general descent south of that band to 30°S. The topographic Rossby wave train generated by westerly winds impinging on the Himalayas may interact with a small region of uplift focused over the Andes in Peru (not shown) when it crosses into the Southern Hemisphere. However, in addition it should be noted that the wave train occurs at a time of seasonal minimum in Southern Hemisphere CO_2.

Question 3

Comments from Referee:

Pg2, Lines 31ff : I strongly believe, these features in C_mlo-cgo should also be shown using other tracers, e.g., SF6, CH4, N2O and halocarbons. The data are available at CSIRO, or NOAA. At the least I would like to see an anslysis using these species in the supplement.

Author's response:

As noted in our first Response to RC1: "We have carried out extra seasonal correlations between the Mauna Loa minus Cape Grim difference in trace gas species (CH_4, CO, H_2, N_2O) routinely monitored by CSIRO with the our dynamical indices. We have also included corresponding correlations using NOAA SF_6 data." This material has now been included as a new Section 6 of the manuscript.

Author's changes to manuscript:

6 Interhemispheric exchange of other trace gases

Next, we consider the eddy and mean IH exchange of other trace gas species and their correlations with CO_2 and dynamical indices of transport. We focus on Feb-Apr for eddy transport and Jun-Aug for mean transport since these periods were the peaks for correlations of CO_2 IH difference with eddy and mean transport indices respectively. However, there are differences in the seasonal variability of interhemispheric gradient in the different trace gas species that are reflected in their transport and for that reason we also briefly mention the results for other time periods. We begin by further examining Mauna Loa minus Cape Grim (mlo–cgo) differences, between 1992-2016, in the routinely monitored CSIRO species CH_4, CO and H_2 in addition to CO_2 that were briefly considered in Frederiksen and Francey (FF16), as well as N_2O (for 1993-2016). Thereafter we discuss mlo–cgo differences in SF_6 data sourced from the NOAA Halocarbons and other Atmospheric Trace Species Group (HATS) program from 1998 (NOAA, 2018).

6.1 Pacific westerly duct and eddy IH transport of CSIRO monitored trace gases

The IH exchange of the trace gas species CH_4, CO and H_2, in addition to CO_2, and the role of the Pacific westerly wind duct was also considered in FF16. In particular, the covariance, of the mlo–cgo difference in these routinely monitored CSIRO species with u_{duct}, is shown in Figure 5 of FF16. We recall that the u_{duct} index is the average zonal wind in the region 5°N to 5°S, 140°W to 170°W at 300hPa. As noted in FF16, the extreme cases of Pacific westerly duct closure in 1997–98 and 2009–10 show up in the reduction of seasonal IH exchange for CH_4 and CO as well as CO_2. The similar behaviour of detrended anomalies of mlo–cgo difference in CH_4, CO and CO_2 and their correlations with u_{duct} is shown in Table 3 for Feb–Apr. We note the quite high correlations of CH_4 and CO with CO_2 ($r = 0.697$ and $r = 0.645$ respectively) and the significant anti–correlations of all these three species with u_{duct} ($r = -0.448$, $r = -0.605$ and $r = -0.500$ respectively). In fact, for Mar-May the correlation between CH_4 and CO_2 is even larger at $r = 0.728$ (and with u_{duct} it is $r = -0.474$) while between CO and CO_2 it is $r = 0.611$ (and with u_{duct} it is $r = -0.507$). These results are of course consistent with Figure 5 of FF16 and are further evidence of similarities of IH transient eddy transport of these three gases. Table 3 also shows that the Feb-Apr correlation of H_2 with CO_2 and anti–correlation with u_{duct} have smaller magnitudes ($r = 0.296$ and $r = -0.218$ respectively) . These results for anomalies are probably related to corresponding similarities and differences in the seasonal mean values (not shown) of these gases in Feb–Apr, as discussed below.

Anomalies in mlo–cgo differences in CSIRO monitored N_2O are generally poorly correlated with those in CO_2 as shown for Feb-Apr and Jun-Aug in Tables 3 and 4 respectively (the maximum 3 month average correlation is $r = 0.274$ for Mar-May) and this is mirrored in generally poor correlation with the dynamical indices shown in Tables 3 and 4. This reflects the fact that natural exchanges with equatorial agriculture and oceans are the main sources (Ishijima et al., 2009), and the seasonal range in mlo-cgo difference is only around 0.2% of the mean N_2O level, more than 10 times less than is the case for the other species.

6.2 Hadley circulation and mean IH transport of CSIRO monitored trace gases

We examine the role of the Hadley circulation on the mean transport of trace gases focusing on the boreal summer period of Jun–Aug. Table 4 shows the correlations between the detrended anomalies of mlo–cgo difference in CH_4, CO and H_2 with CO_2 and with the dynamical indices ω_P and v_P (Table 1). We note that the largest Jun-Aug correlation is between H_2 and CO_2 ($r = 0.680$) and the correlations between CH_4 and CO with CO_2 are considerably smaller ($r = 0.246$ and $r = 0.108$ respectively) while for Apr-Jun the latter correlations are more comparable at $r = 0.583$ and $r = 0.496$ respectively.

These correlations with CO_2 are also reflected in the respective correlations of the other trace gases with ω_P and v_P . We note from Table 4 that the Jun-Aug correlations of H_2 with ω_P and v_P are $r = 0.427$ and $r = 0.442$ respectively which is slightly less than the corresponding correlations between CO_2 and the dynamical indices ($r = 0.522$ and $r = 0.539$ respectively) but considerably larger than for CH_4 and CO. For May-Jul the correlation of H_2 with ω_P is slightly larger with $r = 0.526$.

Again, the different behaviour of the trace gas anomalies may be related to their different seasonal mean values; the seasonal mean IH difference for H_2 peaks in boreal summer while for CH_4 and CO it is relatively low with a minimum in August. The distribution and variability of surface exchange is different for each of the trace gases and there is potential for this to interact with the restricted extent and seasonal meandering of the regions of uplift to influence IH exchange of a species. For example, 70% of the global total CH_4 emissions are from mainly equatorial biogenic sources that include wetlands, rice agriculture, livestock, landfills, forests, oceans and termites (Denman et al., 2007) and CO emissions contain a significant contribution from CH_4 oxidation and from tropical biomass burning.

A more detailed examination of the inter–annual variation of the mlo–cgo difference in H_2 during boreal summer is presented in Figure 8. It shows the detrended H_2 data in comparison with the corresponding CO_2 data and with the ω_P and v_P indices.

First we note that the detrended CO_2 data in the top panel has very similar inter–annual variation to the FF–adjusted $C^*_{mlo\text{-}cgo}$ in Figure 7(b). We also see that the qualitative behaviour of H_2 mirrors many aspects of CO_2, as expected from the correlations in Table 4. In particular, the increase in the IH difference of H_2 in 2010 is even more pronounced than for CO_2. For CO_2 and for H_2 there is a steady reduction in the IH difference from around 2013 leading to a local minimum in 2016. In both of these respects these gases broadly follow the changes in the Hadley circulation including the strengthening during 2015–2016. Vertical lines in Figure 8 indicate other times between 1992 and 2016 when transitions occur in both these trace gases and in the Hadley circulation characterized by ω_P and v_P.

Surface exchanges of H_2 have similarities to those of CO_2 in that they occur mostly at mid–northern latitudes and are mainly due to emissions from Fossil Fuel combustion. However H_2 also has mid–northern latitude photochemical sources peaking in August (Price et al., 2007). These boreal summer sources are almost offset by a combined soil and hydroxyl sink, but the overall interhemispheric partial pressure difference is boosted by a significant reduction in the Southern Hemisphere photochemical source at that time. For both species, the most northern excursions of the inter–tropical convergence zone that occurs at Pacific latitudes encounter increasing concentrations of both gases.

As noted above, anomalies in mlo–cgo differences in N_2O are poorly correlated with those in CO_2 and in dynamical indices (Tables 3 and 4). Indeed the 3 month average anti-correlation with u_{duct} that has the largest magnitude is $r = -0.133$ for Mar-May and the largest correlations with ω_P is $r = 0.359$ for Apr-Jun and with v_P is $r = 0.350$ for May-Jul.

6.3 Interhemispheric exchange of SF_6

In the case of SF6 we have analysed the mlo–cgo difference in available NOAA HATS data from 1998 to 2012 when cgo HATS measurements ceased. Correlations (Tables 3 and 4) of detrended anomalies in IH differences in SF_6 with those in CO_2 are as follows: the Feb–Apr correlation is $r = 0.619$, the Mar-May correlation is $r = 0.722$, the Apr-Jun correlation is $r = 0.595$, the May–Jul correlation is $r = 0.303$ and the Jun–Aug correlation is $r = 0.223$. The corresponding correlations with dynamical indices are as follows: for Feb–Apr the correlation with u_{duct} is $r = -0.617$, the May–Jul correlations with ω_P is $r = 0.465$, the Jun–Aug correlation with ω_P is $r = 0.433$, the May–Jul correlation with v_P is $r = 0.517$ and the Jun–Aug correlation with v_P is $r = 0.385$. We note that SF_6 has an anti-correlation with u_{duct} for Feb-Apr that has larger magnitude than for CO_2 and even CO. Thus, there is again a significant influence of the Pacific westerly duct, in late boreal winter and spring, and of the Hadley circulation, in boreal summer and late spring, as measured by these indices, on the mlo–cgo differences of SF_6; these SF_6 differences exhibit a similar step change in 2009-2010 as shown for CO_2 in Figures 2 and 7.

Unprecedented strength of Hadley circulation in 2015-2016 impacts on CO_2 interhemispheric difference

Jorgen S. Frederiksen and Roger J. Francey

CSIRO Oceans and Atmosphere, Aspendale, Victoria, AUSTRALIA

Correspondence to: Jorgen S. Frederiksen (jorgen.frederiksen@csiro.au)

Response to Anonymous Referee 2 (RC2) review:

We are pleased to learn that the Referee finds our article an interesting study and would like to recommend publishing it in ACP. We thank the Referee for the helpful comments which have helped us in clarifying aspects of the paper and to make it more accessible to the carbon cycle readership. We have responded to the Referee's specific suggestions as follows:

Question 1

Comments from Referee:

You may consider to repeat some more information from FF16. Currently the paper can only be understood when also having read FF16. Also some more background information would help, e.g.: - Can you add a general sentence about Rossby wave dispersion and the mechanism how it transports atmospheric tracers? - Is the interhemispheric "duct" a pre-established concept, or is FF16 the place where it was first introduced? Why is the duct located over oceans only? Is it obvious why Pacific and Atlantic ducts are anti-correlated?
P1 L25: I did not understand the formulation "on the basis of long-term correlations". Why would eddy transport necessarily be expected to correlate with SOI?

Author's response:

At the suggestion of the Referee, we have summarized some more of the dynamical discussion from FF16 to make the current article more self contained. We now discuss the Walker circulation, Rossby wave dispersion, Rossby wave breaking and the associated eddy transport and mixing of atmospheric tracers. We provide additional content on the historical understanding of the westerly ducts, on why the ducts are located over the oceans and why the Pacific and Atlantic ducts are generally anticorrelated. We now discuss the role of the SOI in eddy transport variability (original P1 L25).

Author's changes to manuscript:

On the basis of long-term (1949-2011) correlations of the upper-tropospheric zonal wind with the Southern Oscillation Index (SOI), Francey & Frederiksen (2016; hereafter FF16) defined an index for the Pacific westerly

duct, u_{duct}, as a measure of IH eddy transport of CO_2. This index is the average zonal wind in the region 5°N to 5°S, 140°W to 170°W at 300hPa, as summarized in Table 1. In this article the period of interest is 1992 to 2016 and the corresponding correlation is shown in Figure 1S of the Supplement. There the role of the changing Walker circulation with the cycle of the El Niño-Southern Oscillation (ENSO) in determining the properties of the Pacific and Atlantic westerly ducts is also documented.

SUPPLEMENTARY INFORMATION

1 Pacific and Atlantic westerly ducts

The interhemispheric response to mid-latitude forcing produced by Rossby dispersion through equatorial westerly ducts was documented by Webster and Holton (1982). The zonal winds in the equatorial troposphere are generally easterly but in the upper troposphere the winds may be westerly in the Pacfic duct (centred on 5°N-5°S, 140°W-170°W) or the Atlantic duct (centred on 5°N-5°S, 10°W-40°W) as shown in Figure 2 of Webster and Chang (1988). As discussed in Francey and Frederiksen (2016, denoted FF16), and shown in Figure 1S for the period 1992 to 2016 of interest here, the upper-tropospheric zonal wind is strongly correlated with the SOI in the Pacific duct region and anti-correlated in the Atlantic duct region. As the atmospheric circulation changes between La Niña and El Niño conditions the warm ocean temperatures move from the western to eastern Pacific. The upward branch of the Walker circulation follows the warm water and the associated upper-tropospheric westerlies to the east of the uplift successively open the Pacific westerly duct and then the Atlantic westerly duct (Figure 1 of Webster and Chang 1988). This is the reason for the correlations in our Figure 1S. The strength (and sign) of the upper-tropospheric zonal velocity in the near-equatorial regions is correlated with corresponding levels in the turbulent kinetic energy which is generated by Rossby wave breaking (Figure 6 of Frederiksen and Webster 1988). The Pacific duct, u_{duct} of Table 1, is in general the dominant duct as shown in Figure 2S which depicts the boreal winter (Dec-Feb) vector wind for 1992-2016.

Question 2

Comments from Referee:

Please specify somewhere where the wind data (used to calculate the indices) are taken from (NCEP?). If the winds are taken from re-analysis, a statement of the uncertainty in the upper-troposphere winds would be appropriate, because the study relies on them. How can they be validated?

Author's response:

The wind data is taken from the NCEP-NCAR reanalysis (NNR) data as stated on lines 13 to 15 of page 2 of the original manuscript. We now discuss the accuracy of the upper troposphere winds from NNR and compare our main results with ones based on NASA-MERRA reanalysis data set.

Author's changes to manuscript:

The atmospheric circulation data and indices used throughout this article are obtained from the National Centers for Environmental Prediction (NCEP) and National Center for Atmospheric Research (NCAR) reanalysis (NNR) data (Kalnay et al., 1996); in Section 6 we briefly consider the robustness of our results using another reanalysis data set.

The dynamical indices that we have used for this study are based on the NCEP-NCAR reanalysis (NNR) data (Kalnay et al. 1996). There is generally close correspondence between the major global atmospheric circulation data sets that, like the NNR data, use full data assimilation throughout the atmosphere (Frederiksen & Frederiksen 2007; Frederiksen et al. 2017; Rikus 2018). We have confirmed this by recalculating our dynamical indices and main correlations with $C_{mlo\text{-}cgo}$ based on the NASA Modern Era Retrospective-analysis for Research and Applications (MERRA) (Rienecker et al. 2011) data. For example, the 1992 to 2016 correlation between MERRA and NNR data for u_{duct} in Feb-Apr is $r = 0.974$, for ω_P in Jun-Aug is $r = 0.899$ and for v_P in Jun-

Aug is $r = 0.931$. The corresponding correlations between detrended anomalies of $C_{mlo\text{-}cgo}$ and the MERRA based dynamical indices are also very similar. The correlations are $r = -0.512$ with u_{duct} for Feb-Apr (compared with $r = -0.500$ for the NNR index), $r = 0.504$ with ω_P for Jun-Aug (compared with $r = 0.522$ based on NNR) and $r = 0.538$ with v_P for Jun-Aug (compared with $r = 0.539$ based on NNR).

Question 3

Comments from Referee:

P2 L10: What does "uses the overlap" mean? This needs an explicit description.
Same paragraph: Add the year (always 2015?) to all dates given.

Author's response:

The sentence referring to "uses the overlap" has been rewritten (original P2 L10). The year 2015 has been added to all the dates.

Author's changes to manuscript:

Requested changes implemented.

Question 4

Comments from Referee:

P3 L8: "Modelling" is a very broad term, that could mean anything. Please add a brief description what has been done (e.g. saying "atmospheric transport simulation" with a description of the CO2 fluxes used). Reading FF16 did not actually clarify to me what you refer to here.

Author's response:

The sentence starting "Modelling" has been deleted and replaced by a much more detailed discussion also at the request of RC1 and RC3.

Author's changes to manuscript:

2.1 The influences of terrestrial fluxes and transport on interhemispheric CO_2 differences

The growth rate and concentration of atmospheric CO_2 depend on many mechanisms including fossil fuel emissions, surface fluxes, such as associated with the growth and decay of vegetation, and atmospheric mean and eddy transport. The CO_2 growth rate and IH gradients in CO_2 vary on daily, monthly, yearly and multi-year time scales where there is a quasi-periodic variability associated with the influence of ENSO (e.g. Thoning et al. 1989). This reflects the response of tropical vegetation to rainfall variations and both hemispheres are also affected through dynamical coupling.

A number of recent inversion studies have largely attributed growth anomalies in atmospheric CO_2 concentrations to anomalous responses of the terrestrial biosphere. However, the variability in the responses within Dynamic Global Vegetation Models (DGVMs) is significant. Le Quéré et al. (2017) for example note that the "standard deviation of the annual CO_2 sink across the DGVMs averages to ± 0.8 GtC yr^{-1} for the period 1959 to 2016". This is significantly larger than the reported extratropical sink anomalies during for example the major 2009-2010 step in CO_2 concentrations (Poulter et al., 2014; Trudinger et al., 2016). Francey and Frederiksen (2015) presented reasons supporting a dynamical contribution to the cause of the 2009-2010 $C_{mlo\text{-}cgo}$ step.

For the 2015-2016 period of particular relevance here there are two studies that stand out. Keenan et al. (2016) interpret slowing CO_2 growth in 2016 as strong uptake by Northern Hemisphere terrestrial forests. Yue et al. (2018) examine the reasons for the strong positive anomalies in atmospheric CO_2 growth rates during 2015. They present evidence of the Northern Hemisphere terrestrial response to El Niño events by way of satellite observations of vegetation greenness. To reconcile increased greenness with increased CO_2 growth their

inversion modelling requires the “largest ever observed” transition from sink to source in the tropical biosphere at the peak of the El Niño, “but the detailed mechanisms underlying such an extreme transition remain to be elucidated”.
In this study, we find that the 2015-2016 El Niño also corresponds to unprecedented anomalies in both mean and eddy IH CO_2 transport characterized by indices of these transfers that we introduce, affecting Northern Hemisphere CO_2 growth. As for the anomalies in CO_2 IH gradient during the 2009-2010 El Niño, studied in FF16, this again suggests a contributing role for anomalous IH transport during the 2015-2016 event. We examine this possibility in detail and study the relationships between the extremes in IH CO_2 differences and transport anomalies for 1992 to 2016 and associated correlations between $C_{mlo\text{-}cgo}$ (and other trace gases) and dynamical indices of transport.

Question 5

Comments from Referee:
P3 L25: It would help (here and at various other places) to split long sentences by commas, here e.g. after "15N", for a faster perception which parts belong together. (Also, e.g., P4 L8 after "wind" and "(140W-170W)", P8 L20 after "duct", P8 L26 after "open".) P5 L22-24: I found this sentence unclear. Maybe "with" in line 22 should be "which"?

Author’s response:

Here (original P3 L21 to L24) and elsewhere long sentences have been split as suggested. This sentence (original P5 L22-24) has been rewritten.

Author’s changes to manuscript:

Requested changes implemented.

Question 6

Comments from Referee:
Sect 5: I would find it interesting to know which fraction of interannual variability in Cmlo−cgo can be explained by transport variability alone? Is it r^2 = 25%? (In addition, I found the description of the correlation analysis not easy to follow, e.g. with respect to the two quantities C and C*.)

Author’s response:

Yes, as the Referee notes, typically the correlations of MLO-CGO CO_2 with our indices that explain transport have $|\boldsymbol{r}| = \mathbf{0.5}$ or slightly larger. The relationships between C and C* are further discussed and related to a new Figure.

Author’s changes to manuscript:
In fact the FF-adjusted $C^*_{mlo\text{-}cgo}$ has very similar behaviour to the detrended $C_{mlo\text{-}cgo}$, with pattern correlations of anomalies of $r = 0.931$, $r = 0.954$ and $r = 0.981$ for Jan-Dec, Jun-Aug and Feb-Apr respectively. The similarity can also be seen by comparing the top panel of Figure 7(b) with that of Figure 8.

Question 7

Comments from Referee:

P7 L7-8: Briefly say where the information on anomalously high/low NBP is coming from (biosphere model? eddy covariance data?).

Author's response:

Reference is now given to Trudinger et al. (2016) where the details are given and that work is also discussed in Section 2.1 referred to in the response to Question 4.

Author's changes to manuscript:

Terrestrial Net Biosphere Production south of 30°S was also anomalously low in 2009 and anomalously high in 2010 (FF16; Trudinger et al. 2016; though by amounts not sufficient to impact on the Cape Grim baseline CO_2 records).

Question 8

Comments from Referee:

P7 L11: Is "indicated" the right word here? Do you mean "connected"?
P8 L28-31: De-compact the formulations, e.g. saying "vertical velocity w at 300hPa" (and again comma after 15N)
Fig 1a: Unclear what the inset "OCO-2 Satellite" refers to in the graphics.
Fig 5: The labelling is much too small to be readable. Also, it would be helpful to add row and column headings to the panels.

Author's response:

These sentences have been rephrased, "OCO-2 Satellite" has been explained and the Figures have been improved with row and column headings.

Author's changes to manuscript:

Rephrasing implemented.
Figure 1: (a) OCO-2 image for 17 Feb 2015 showing Rossby wave dispersion (dashed red lines) in CO_2 concentration across the equator (dotted black line); the box labeled 'OCO-2 Satellite' shows the time period of the associated movie, (b) seasonal cycle of $C_{mlo\text{-}cgo}$ and u_{duct}, with area where both are positive shaded, for 1 Jan 2014 to 31 Dec 2016, and (c) 300 hPa wind vector directions and wind strength (ms^{-1}) on 17 Feb 2015.
Figures all updated.

Unprecedented strength of Hadley circulation in 2015-2016 impacts on CO_2 interhemispheric difference

Jorgen S. Frederiksen and Roger J. Francey

CSIRO Oceans and Atmosphere, Aspendale, Victoria, AUSTRALIA

Correspondence to: Jorgen S. Frederiksen (jorgen.frederiksen@csiro.au)

Response to AC Chatterjee Referee 3 (RC3) review:

We are pleased to learn that the Referee thinks that the publication in ACP of this study, connecting the large-scale dynamics to observed variations in atmospheric CO_2 concentrations, would be timely. We thank the Referee for the insightful comments which have led us to clarify and improve the presentation of the results and to add more detailed discussion on surface flux variability. To be specific, we have responded to the Referee's suggestions as follows:

Question 1

Comments from Referee:

The observed interannual variability in Cmlo-cgo has to be a function of both the transport variability and the underlying surface flux variability. This latter part, especially the role of terrestrial ecosystems during the boreal summer-autumn is largely ignored. For example, in Section 4 (Lines 22-24) the authors talk about the impact of fossil fuel emissions over NH but do not counteract that with the strong biospheric uptake that happen at the same time. I would recommend that the authors have a discussion at the outset on how they are considering surface flux variability in their analyses. In the current version of the manuscript, this is not clear at all.

Author's response:

We agree with the Referee that interannual variability in $C_{mlo-cgo}$ has to be a function of both transport variability and the underlying surface flux variability. Our focus has been to point out, in FF16 and in the current study, that transport variability may, at certain times, be an additional important contributor. We have followed the Referee's suggestion and added at the outset a new Subsection 2.1 on extratropical terrestrial flux variation.

Author's changes to manuscript:

2.1 The influences of terrestrial fluxes and transport on interhemispheric CO_2 differences

The growth rate and concentration of atmospheric CO_2 depend on many mechanisms including fossil fuel emissions, surface fluxes, such as associated with the growth and decay of vegetation, and atmospheric mean and eddy transport. The CO_2 growth rate and IH gradients in CO_2 vary on daily, monthly, yearly and multi-year time scales where there is a quasi-periodic variability associated with the influence of ENSO (e.g. Thoning et al. 1989). This reflects the response of tropical vegetation to rainfall variations and both hemispheres are also affected through dynamical coupling.

A number of recent inversion studies have largely attributed growth anomalies in atmospheric CO_2 concentrations to anomalous responses of the terrestrial biosphere. However, the variability in the responses within Dynamic Global Vegetation Models (DGVMs) is significant. Le Quéré et al. (2017) for example note that the "standard deviation of the annual CO_2 sink across the DGVMs averages to ± 0.8 GtC yr^{-1} for the period 1959 to 2016". This is significantly larger than the reported extratropical sink anomalies during for example the major 2009-2010 step in CO_2 concentrations (Poulter et al., 2014; Trudinger et al., 2016). Francey and Frederiksen (2015) presented reasons supporting a dynamical contribution to the cause of the 2009-2010 $C_{mlo-cgo}$ step.

For the 2015-2016 period of particular relevance here there are two studies that stand out. Keenan et al. (2016) interpret slowing CO_2 growth in 2016 as strong uptake by Northern Hemisphere terrestrial forests. Yue et al. (2018) examine the reasons for the strong positive anomalies in atmospheric CO_2 growth rates during 2015. They present evidence of the Northern Hemisphere terrestrial response to El Niño events by way of satellite observations of vegetation greenness. To reconcile increased greenness with increased CO_2 growth their inversion modelling requires the "largest ever observed" transition from sink to source in the tropical biosphere at the peak of the El Niño, "but the detailed mechanisms underlying such an extreme transition remain to be elucidated".

In this study, we find that the 2015-2016 El Niño also corresponds to unprecedented anomalies in both mean and eddy IH CO_2 transport characterized by indices of these transfers that we introduce, affecting Northern Hemisphere CO_2 growth. As for the anomalies in CO_2 IH gradient during the 2009-2010 El Niño, studied in FF16, this again suggests a contributing role for anomalous IH transport during the 2015-2016 event. We examine this possibility in detail and study the relationships between the extremes in IH CO_2 differences and transport anomalies for 1992 to 2016 and associated correlations between $C_{mlo-cgo}$ (and other trace gases) and dynamical indices of transport.

Question 2

Comments from Referee:

Since the authors examine the IH CO2 annual difference from 1992 through to 2016, it is curious that the authors don't attempt to put their findings for the 2015-2016 El Niño in context of the 1997-1998 El Niño. Figure 6 indicates that the eddy transport may have placed a larger role in the IH CO2 annual difference relative to the mean transport. This raises a bigger question - each El Niño has its own unique flavor, thus giving rise to its own individual teleconnection patterns (see Capotondi et al. [2015] BAMS, also available here - http://ocean.eas.gatech.edu/manu/papers/PDFs/Capotondi-2015-Understanding-ENSO-Diversity.pdf], it will be great to see a brief summary/discussion of how different El Niño flavors, and potentially a shift in El Niño type (EP – to – CP El Niños) may impact the two transport indices.

Author's response:

We thank the Referee for the reference to Capotondi et al. (2015) which is now referred to. We now also discuss the 1997-1998 El Niño, El Niño flavours and in particular the differences in the Hadley circulation and in global warming between 1997-1998 and 2015-2016.

Author's changes to manuscript:

The somewhat different behaviours of $C_{mlo-cgo}$ and the dynamical indices, particularly during the El Niños of 2009-2010 and 2015-2016 and of 1997-1998, may partly reflect the diversity of El Niños and whether the heating is focussed in the Eastern Pacific or in the Central Pacific (Capotondi et al. 2015; L'Heureux et al. 2017 and references therein). The strong 1997-1998 event, like the 1982-1983 event, was a classic Eastern Pacific El Niño with maximum temperature anomalies there of nearly $+4^{o}$ C (L'Heureux et al. 2017). The 2009-2010 event in contrast was a Central Pacific El Niño with record-breaking warming in the central Pacific (Kim et al. 2011). The 2015-2016 El Niño fell between these two canonical cases with less warming in the eastern Pacific Ocean than the 1997-1998 event but similar warming to the 2009-2010 event in the central Pacific (L'Heureux et al. 2017).

The broadly increasing magnitude of the negative ω and v indices since 2012 is associated with both increasing global temperatures, breaking the record in 2016, and the large El Niño of 2015 and 2016. This has resulted in

the increasing importance of the mean convective and advective CO_2 transport by the Hadley circulation relative to the eddy transport including through the Pacific duct.

Question 3

Comments from Referee:

The authors heavily rely on the information from the Francey and Frederiksen [2016] paper, especially in the discussion about the Atlantic duct (Section 3.1). The authors may want to include the relevant figure in this paper or introduce the necessary concepts here as well. Currently, it is challenging to put this paper in context without going back and reading the 2016 paper (which is what I had to do). For example, in Section 2, the authors talk about modeling that was done in FF16 – it is impossible to know what kind of modeling was done. It is possible to reduce the dependence on that paper by introducing the concepts about the Pacific, Atlantic duct early on and providing a short summary of the findings. In a lot of places, reference to FF16 is not necessary.

Author's response:

At the suggestion of the Referee, we have summarized some more of the dynamical discussion from FF16 to make the current article more self contained. Also as noted in relation to Question 1 a new subsection has been added that details the modelling.

Author's changes to manuscript:

On the basis of long-term (1949-2011) correlations of the upper-tropospheric zonal wind with the Southern Oscillation Index (SOI), Francey & Frederiksen (2016; hereafter FF16) defined an index for the Pacific westerly duct, u_{duct}, as a measure of IH eddy transport of CO_2. This index is the average zonal wind in the region 5°N to 5°S, 140°W to 170°W at 300hPa, as summarized in Table 1. In this article the period of interest is 1992 to 2016 and the corresponding correlation is shown in Figure 1S of the Supplement. There the role of the changing Walker circulation with the cycle of the El Niño-Southern Oscillation (ENSO) in determining the properties of the Pacific and Atlantic westerly ducts is also documented.

SUPPLEMENTARY INFORMATION

1 Pacific and Atlantic westerly ducts

The interhemispheric response to mid-latitude forcing produced by Rossby dispersion through equatorial westerly ducts was documented by Webster and Holton (1982). The zonal winds in the equatorial troposphere are generally easterly but in the upper troposphere the winds may be westerly in the Pacfic duct (centred on 5°N-5°S, 140°W-170°W) or the Atlantic duct (centred on 5°N-5°S, 10°W-40°W) as shown in Figure 2 of Webster and Chang (1988). As discussed in Francey and Frederiksen (2016, denoted FF16), and shown in Figure 1S for the period 1992 to 2016 of interest here, the upper-tropospheric zonal wind is strongly correlated with the SOI in the Pacific duct region and anti-correlated in the Atlantic duct region. As the atmospheric circulation changes between La Niña and El Niño conditions the warm ocean temperatures move from the western to eastern Pacific. The upward branch of the Walker circulation follows the warm water and the associated upper-tropospheric westerlies to the east of the uplift successively open the Pacific westerly duct and then the Atlantic westerly duct (Figure 1 of Webster and Chang 1988). This is the reason for the correlations in our Figure 1S. The strength (and sign) of the upper-tropospheric zonal velocity in the near-equatorial regions is correlated with corresponding levels in the turbulent kinetic energy which is generated by Rossby wave breaking (Figure 6 of Frederiksen and Webster 1988). The Pacific duct, u_{duct} of Table 1, is in general the dominant duct as shown in Figure 2S which depicts the boreal winter (Dec-Feb) upper tropospheric vector wind for 1992-2016.

Question 4

Comments from Referee:

Overall quality of the text and figures: A couple of figures need to be improved, especially Figures 1 and 5. Either the figure resolution is low or it is too hard to read the figures. For the NASA movie, the authors may

want to check the appropriate procedure to reference a video animation. The authors also need to provide the necessary credits to NASA Goddard Space Flight Center and the production team, including the URL for the movie (see https://svs.gsfc.nasa.gov/12445).

Author's response:

We have improved the clarity of the labelling on several of the figures including Figures 1 and 5 (which has been split into the new Figures 5 and 6). We have also credited the NASA Goddard Space Flight Center and the production team and referenced the URL for the movie as suggested by the Referee.

Author's changes to manuscript:

Please see new Figures and Captions.
We acknowledge NASA Goddard Flight Center and their Production Team for the movie 'Following Carbon Dioxide through the Atmosphere' available at the web site: https://svs.gsfc.nasa.gov/12445.

Question 5

Comments from Referee:

Minor/technical comments: a) Abstract – Line 15-16 – incomplete line b) Section 3.2, Lines 3 - 6 – it is not clear how Figure 4 captures the convective transport of CO2 emissions. Later the authors claim – "It demonstrates that when the Pacific duct is open there is also large-scale uplift slightly downstream of Asia, so. . .". It is not clear how all this information is derived from Figure 4. c) Throughout the manuscript, the authors introduce the different transport indices in line (i.e., in the text). Given that this paper will be of significant interest to the carbon cycle community (and several of whom may not be familiar with these notations), it may be useful to have a Table that introduces the notation, what it means/represents and how it is calculated. d) The overall text requires some careful and thorough editing. Several sentences are hard to read either due to a lack of punctuation or overuse of conjunctive adverbs.

Author's response:

We have attended to the minor – technical comments. We now note that the prominent correlations shown in Figure 4, within ±30°of the equator at longitudes 120°E to 170°W, in fact occur at all levels between the surface and 100 hPa. We have added a table summarizing the definitions of the transport indices. The text has been carefully edited and sentences split for clarity.

Author's changes to manuscript:

The most prominent correlations occur within ±30°of the equator at longitudes 120°E to 170°W, upstream and at the longitudes of the Pacific duct and this is in fact the case at all levels between the surface and 100 hPa (not shown). Broadly similar correlations are obtained between the 500 hPa ω and u_{duct} for Feb-Apr (and for 500 hPa ω and SOI for Jan-Dec).

Table 1: Definitions of dynamical indices characterizing eddy and mean tracer transport.

Dynamical index	Definition
u_{duct}	Average 300 hPa zonal velocity in the region 5°N to 5°S, 140°W to 170°W.
ω_H	Average 300 hPa vertical velocity in pressure coordinates in the region 10°N to 15°N, 0 to

	360E.
v_P	Average 200 hPa meridional velocity in the region 5°N to 10°N, 0 to 360E.
ω_P	Average 300 hPa vertical velocity in pressure coordinates in the region 10°N to 15°N, 120E to 240E.
v_H	Average 200 hPa meridional velocity in the region 10°N to 15°N, 120E to 240E.

Unprecedented strength of Hadley circulation in 2015-2016 impacts on CO_2 interhemispheric difference

Jorgen S. Frederiksen and Roger J. Francey

CSIRO Oceans and Atmosphere, Aspendale, Victoria, AUSTRALIA

Correspondence to: Jorgen S. Frederiksen (jorgen.frederiksen@csiro.au)

Abstract. The extreme El Niño of 2015 and 2016 coincided with record global warming and unprecedented strength of the Hadley circulation with significant impact on mean interhemispheric (IH) transport of CO_2 ~~and on the difference in CO_2 concentration between Mauna Loa and Cape Grim ($C_{mlo-cgo}$)~~. The relative roles of eddy transport and mean advective transport on ~~IH CO_2~~ interannual differences in CO_2 concentration between Mauna Loa and Cape Grim ($C_{mlo-cgo}$), from 1992 through to 2016, are~~is~~ explored. Eddy transport processes occur mainly in boreal winter-spring when $C_{mlo-cgo}$ is large; an important component is due to Rossby wave generation by the Himalayas and propagation through the equatorial Pacific westerly duct generating and transmitting turbulent kinetic energy. Mean transport occurs mainly in boreal summer-autumn and varies with the strength of the Hadley circulation. The timing of annual changes in $C_{mlo-cgo}$ is found to coincide well with dynamical indices that we introduce to characterize the transports. During the unrivalled 2009-2010 step in $C_{mlo-cgo}$ ~~indices~~ the effects of the eddy and mean transport reinforce. In contrast for the 2015 to 2016 change in $C_{mlo-cgo}$ the mean transport counteracts the eddy transport and the record strength of the Hadley circulation determines the annual IH CO_2 difference. The interaction of increasing global warming and extreme El Niños may have important implications for altering the balance between eddy and mean IH CO_2 transfer. The effects of interannual changes in mean and eddy transport on interhemispheric gradients in other trace gases are also examined.

1 Introduction

Interhemispheric (IH) exchange of CO_2 occurs mainly by eddy transport in the boreal winter-spring and by mean convective and advective exchange in the boreal summer-autumn (Bowman and Cohen, 1997; Lintner et al., 2004; Miyazaki et al. 2008; and references therein).

On the basis of long-term (1949-2011) correlations of the upper-tropospheric zonal wind with the Southern Oscillation Index (SOI), Francey & Frederiksen (2016; hereafter FF16) defined an index for the Pacific westerly duct, u_{duct}, as a measure of IH eddy transport of CO_2. This index is the average zonal wind in the region 5°N to 5°S, 140°W to 170°W at 300hPa, as summarized in Table 1. In this article the period of interest is 1992 to 2016 and the corresponding correlation is shown in

Figure 1S of the Supplement. There the role of the changing Walker circulation with the cycle of the El Niño-Southern Oscillation (ENSO) in determining the properties of the Pacific and Atlantic westerly ducts is also documented. ~~It~~ The u_{duct} index is an indicator of cross equatorial Rossby wave dispersion and associated increases in near equatorial upper tropospheric transient kinetic energy (Frederiksen and Webster, 1988), particularly between 300 and 100hPa (~9 km to ~16 km above sea level). The process normally occurs over the eastern Pacific Ocean during the boreal winter-spring and the Rossby waves (Webster and Holton, 1982; Stan et al., 2017), generated downwind of thermal anomalies and continental influences, in particular the massive Himalayan orography, propagate in a south-east~~erly~~ direction through the Pacific westerly duct generating and transporting turbulent kinetic energy. The generation of turbulent kinetic energy occurs through Rossby wave breaking in the Pacific and Atlantic ducts and enhances turbulent mixing (Ortega et al. 2018 and references therein). FF16 also considered the relationship of u_{duct} and other trace gases including CH_4. Indeed, recently Pandey et al. (2017) and Knol et al. (2017) also considered the implications of faster IH transfer of CH_4 during the La Niña of 2011 when the Pacific westerly wind duct is open and u_{duct} is large.

FF16 explained the exceptional step in CO_2 IH difference between 2009 and 2010 as due to a contribution from the large anomaly in u_{duct} observed at the time. Recently results from the National Aeronautics and Space Administration (NASA) Orbiting Carbon Observatory-2 (OCO-2) during the 2015-2016 El Niño have been published (Chatterjee et al., 2017; and references therein) ~~and in~~ In particular release by NASA (2016) of data in a movie 'Following Carbon Dioxide through the Atmosphere' provides further direct evidence of the Pacific duct hypothesis. ~~Figure 1a uses the overlap between CO_2 and u_{duct} in early 2015, indicated by shading, to predict IH CO_2 exchange through the Pacific duct.~~ The NASA OCO-2 CO_2 concentration in Figure 1~~b~~(a) is for 17 Feb 2015 and shows Rossby wave trains over the eastern Pacific and across South America associated with IH exchange as a typical example of OCO-2 images that coincide with the shaded 2015 period in Figure 1~~a~~(b). The dynamical properties of these Rossby waves are further explored in the Supplement including Figures 3S and 4S. Figure 1(b) uses the covariance between CO_2 and u_{duct} in early 2015, indicated by shading, to predict IH CO_2 exchange through the Pacific duct. ~~This is also consistent with (u, v) wind vectors~~ The atmospheric circulation data and indices used throughout this article are obtained from the National Centers for Environmental Prediction (NCEP) and National Center for Atmospheric Research (NCAR) reanalysis (NNR) data (Kalnay et al., 1996); in Section 6 we briefly consider the robustness of our results using another reanalysis data set. The results in Figures 1(a) and (b) are also consistent with upper-tropospheric (u, v) wind vectors. Between 5 and 23 February 2015 NNR wind vectors show that a strong Pacific North American height anomaly caused a split in the Pacific upper tropospheric winds, the Pacific westerly duct was open, and there were south-east cross equatorial winds from the Northern to Southern Hemispheres~~;~~. ~~this~~ This is illustrated in Figure 1(c) for 300 hPa wind vectors on 17 Feb 2015.

The focus here is on IH CO_2 difference, anomalies in the mean convective and advective mode of IH CO_2 exchange and changes in the relative importance of the mean and eddy transport modes.

2 Changes in CO_2 interhemispheric difference

To represent CO_2 interhemispheric difference we define $C_{mlo-cgo}$ as the difference in Commonwealth Scientific and Industrial Research Organisation (CSIRO) analysed CO_2 concentrations in baseline air sampled from Mauna Loa (mlo, 20°N, 156°W) and Cape Grim (cgo, 41°S, 145°E). FF16 discussed the measurement and sampling strategy, consistently applied over 25 years, which has been used to establish the data set with minimum uncertainty. They also examined CO_2 interhemispheric difference using NOAA data (Dlugokencky et al. 2014) and with the Scripps Institution of Oceanography (SIO) Mauna Loa and South Pole data (Keeling et al., 2009) and found broad agreement in the two data sets, in the period of overlap since the 1990s, in terms of CO_2 changes and the relationships to the opening and closing of the Pacific westerly duct.

Figure 2 summarises annual covariations that motivated this study. In Figure 2(a) the overall trend in the $C_{mlo-cgo}$ reflects the increasing emissions, mainly in the Northern Hemisphere, of carbon from combustion of fossil fuels coupled with relatively slow transport into the Southern Hemisphere. The smooth dashed curve shows global annual anthropogenic emissions (Le Quere et al., 2017) scaled by the coefficients of linear regression between $C_{mlo-cgo}$ and emissions from 1992-2015 (0.36 ppm/PgC.yr^{-1}, n=24, r^2=0.83). The year-to-year variations in $C_{mlo-cgo}$ are more pronounced than the variations in emissions (for example only 2009, corresponding to the Global Financial Crisis, clearly interrupts the smooth emissions increase).

~~Measurement error and sampling bias are effectively suppressed in this data set, so reasons for variations in $C_{mlo-cgo}$ are sought in non-equatorial surface flux anomalies or variations in interhemispheric exchange. The influences of the major non-equatorial climate forcing on the terrestrial biosphere, the 2002-2003 drought (Cias et al., 2005) and fires (Rayner et al., 2008) in the Northern Hemisphere and the end of the millennium drought in the Southern Hemisphere (Poulter et al., 2014), are not prominent in Figure 2a. Modelling (FF16) confirms that these peak uptakes are generally too small to impact on the Cape Grim baseline record. For this reason this paper focuses on interhemispheric exchange variation.~~

2.1 The influences of terrestrial fluxes and transport on interhemispheric CO_2 differences

The growth rate and concentration of atmospheric CO_2 depend on many mechanisms including fossil fuel emissions, surface fluxes, such as associated with the growth and decay of vegetation, and atmospheric mean and eddy transport. The CO_2 growth rate and IH gradients in CO_2 vary on daily, monthly, yearly and multi-year time scales where there is a quasi-periodic variability associated with the influence of ENSO (e.g. Thoning et al. 1989). This reflects the response of tropical vegetation to rainfall variations and both hemispheres are also affected through dynamical coupling.

A number of recent inversion studies have largely attributed growth anomalies in atmospheric CO_2 concentrations to anomalous responses of the terrestrial biosphere. However, the variability in the responses within Dynamic Global Vegetation Models (DGVMs) is significant. Le Quéré et al. (2017) for example note that the "standard deviation of the annual CO_2 sink across the DGVMs averages to ± 0.8 GtC yr^{-1} for the period 1959 to 2016". This is significantly larger than the reported extratropical sink anomalies during for example the major 2009-2010 step in CO_2 concentrations (Poulter et al.,

2014; Trudinger et al., 2016). Francey and Frederiksen (2015) presented reasons supporting a dynamical contribution to the cause of the 2009-2010 $C_{mlo\text{-}cgo}$ step.

For the 2015-2016 period of particular relevance here there are two studies that stand out. Keenan et al. (2016) interpret slowing CO_2 growth in 2016 as strong uptake by Northern Hemisphere terrestrial forests. Yue et al. (2018) examine the reasons for the strong positive anomalies in atmospheric CO_2 growth rates during 2015. They present evidence of the Northern Hemisphere terrestrial response to El Niño events by way of satellite observations of vegetation greenness. To reconcile increased greenness with increased CO_2 growth their inversion modelling requires the "largest ever observed" transition from sink to source in the tropical biosphere at the peak of the El Niño, "but the detailed mechanisms underlying such an extreme transition remain to be elucidated".

In this study, we find that the 2015-2016 El Niño also corresponds to unprecedented anomalies in both mean and eddy IH CO_2 transport characterized by indices of these transfers that we introduce that affect Northern Hemisphere CO_2 growth. As for the anomalies in CO_2 IH gradient during the 2009-2010 El Niño, studied in FF16, this again suggests a contributing role for anomalous IH transport during the 2015-2016 event. We examine this possibility in detail and study the relationships between the extremes in IH CO_2 differences and transport anomalies for 1992 to 2016 and associated correlations between $C_{mlo\text{-}cgo}$ (and other trace gases) and dynamical indices of transport.

2.2 Dynamical influences on IH exchange

Figure 2(b) confirms that much of the year-to-year variability in $C_{mlo\text{-}cgo}$, particularly preceding 2010, occurs in the boreal winter-spring (Dec-May) when eddy transport is expected to be the more active contribution to IH exchange (FF16). The step jump in annual values between 2009 and 2010 that was the focus of FF16, is the most prominent feature. A similar relationship with u_{duct} is supported prior to 2010 as indicated here by vertical dashed gridlines aligned with the beginning of the calendar years when u_{duct} is unusually low ($u_{duct} \leq 3ms^{-1}$). At these times u_{duct} generally corresponds to above-average $C_{mlo\text{-}cgo}$, consistent with an accumulation of CO_2 in the Northern Hemisphere at a time when the Pacific duct transfer is small.

A notable exception occurs in 2015-2016 and this is a particular focus of this study that we address in the context of the unusual $C_{mlo\text{-}cgo}$ behaviour since 2010. For example, since 2010 the annual average $C_{mlo\text{-}cgo}$ in Figure 2(a) shows reduced scatter and a slight decrease at a time when fossil fuel emissions continue to grow. As shown in Figure 2(b), this $C_{mlo\text{-}cgo}$ decrease is more marked in the boreal summer-autumn (Jun-Nov) than in boreal winter-spring (Dec-May) when it is relatively stable (and even recovers in the last 3 years).

The steadily decreasing u_{duct} since 2012 occurs all year round in Figure 2~~c~~(c). Similar but more marked decreases occur in indices ω_H and v_H in Figure 2(d), which measure the strength and location of the Hadley circulation. Here, ω_H is the 300 hPa vertical velocity in pressure coordinates ($\omega = dp/dt$ where p is pressure) averaged zonally (0-360°) and between 10°N and 15°N (Table 1). ~~And~~ Also, v_H is the 200 hPa south-to-north meridional wind averaged zonally and between 5°N and 10°N (Table 1). Both ω_H and v_H ~~both~~ become more negative and the mean transport from the Northern to Southern

Hemispheres increases with a strengthening of the Hadley circulation. As noted by Freitas et al. (2017; and references therein) the Hadley circulation strengthens during El Niños, and particularly for strong events such as during 2015-2016 (L'Heureux et al., 2017). There are subtle relationships between the latitudinal width of the equatorial heating during El Niño and global warming (Freitas et al., 2017) and the Hadley circulation. However, it is expected that there will be an increasing frequency of extreme El Niño events with increasing global warming (Cai et al., 2014; Yeh et al., 2018).

Before examining the Hadley component further, we clarify factors associated with the eddy transfer through the Pacific duct.

3 The role of the Pacific westerly duct in IH CO_2 eddy transport

We examine here the concept of relatively rapid interhemispheric CO_2 exchange through a spatially restricted Pacific duct and discuss issues of the uniqueness of the duct and the transport of both turbulent kinetic energy and CO_2 to and through the Pacific duct region.

3.1 Eddy generation in the equatorial zone

The u_{duct} zonal wind based on the peak climatological correlation with SOI (140°W -170°W) is also largely representative of near equatorial (5°N to 5°S) zonal winds and their variability in the larger region between 90°W and 180°. Pattern correlations between the two vary from r ~ 0.9 for November to April to r ~ 0.7 for May to October.

In Figure 3, Hovmoller diagrams for the ~~Eastern~~ Western Hemisphere (180° to 0°W) between 2008 and 2016 show the time-longitude of daily 300hPa zonal winds between 5°N and 5°S. The cool blue background represents easterly winds (negative u) while warm colours, green to yellow through to red, depict westerlies (positive u). Frederiksen and and Webster (1988) found that near equatorial upper tropospheric transient kinetic energy generation is approximately linearly related to zonal wind strength (their Figure 6) and is strongest for westerlies when the winds oppose the earth's rotation. The longitudinal limits of u_{duct} determined from the SOI correlation are enclosed by solid white rounded rectangles in Figure 3, while the time period (rectangle height) represents those months when $C_{mlo\text{-}cgo}$ is at a seasonal maximum and winds in the Pacific duct are normally westerly (Feb-Apr).

In most years, u_{duct} is positive in boreal winter-spring and Rossby waves generated by, for example, the Himalayas (height of 8.8 km) can propagate through the downstream Pacific duct region (140°W -170°W, 5°N-5°S) producing and transporting turbulent kinetic energy southwards. In some years, such as the boreal winter-spring of 2009-2010 and 2015-2016, u_{duct} is anomalously weak and the peak equatorial 300 hPa zonal winds are over the Atlantic ocean, particularly in the Atlantic duct region defined as 10°W-40°W, 5°N-5°S. The Atlantic duct region, most conspicuously, is downstream of the Rockies (height of 4.4 km). Figure 1S of our Supplement and Figure 4(a) of FF16 show~~s~~ that the SOI and Atlantic duct zonal winds

are strongly *anti-correlated* in contrast to the strong correlation with u_{duct}; as well, in the ~~Western~~ Eastern Hemisphere the correlation between the SOI and equatorial zonal winds is quite weak. We note that u_{duct} and the Atlantic duct winds are anti-correlated with $r = -0.66$. Further while u_{duct} is anti-correlated with $C_{mlo\text{-}cgo}$ the Atlantic duct winds are correlated with a similar magnitude. This indicates that changes in u_{duct} are the primary determinant of interhemispheric CO_2 duct transfer via eddy processes and $C_{mlo\text{-}cgo}$ and the opening of the Atlantic duct is mainly important through the associated closing of the Pacific duct. This is consistent with the idea that Rossby wave dispersion from the smaller topographic features of the Rockies is less important than from the more massive Himalayas, as further discussed in the Supplement.

3.2 Transport of surface CO_2 emissions to the upper troposphere

Transport of CO_2 emissions from the surface to the upper troposphere is explored ~~in Figure 4~~ next. ~~It demonstrates~~ We find that when the Pacific duct is open there is also large scale uplift slightly downstream of Asia so that in a given winter-spring season the substantial regional emissions are effectively transported directly through the duct via Rossby wave dispersion, including by the Himalayan wave train. Figure 4 shows the Feb-Apr correlation between the 500hPa ω (the vertical wind in pressure coordinates with negative values corresponding to uplift in height coordinates) and the SOI from 1948 to 2016. The most prominent correlations occur within ±30°of the equator at longitudes 120°E to 170°W, upstream and at the longitudes of the Pacific duct and this is in fact the case at all levels between the surface and 100 hPa (not shown). Broadly similar correlations are obtained between the 500 hPa ω and u_{duct} for Feb-Apr (and for 500 hPa ω and SOI for Jan-Dec). At other times, for example in 2010 and 2015-2016, when there have been persisting easterlies in the Pacific duct region there has been descent slightly downstream of the Asian region. Thus the recent record Asian emissions may play a significant role in direct episodic IH CO_2 transfer through the Pacific duct. To the extent that Asian emissions might be preferentially represented in direct IH CO_2 transfer, it is relevant that uncertainty and possibly variability in Asian emissions are greater than the reported uncertainty and variability in the global totals (Andres et al., 2014).

4 The role of the Hadley circulation in mean IH CO_2 transport

As noted in Section 2, the years 2010 and 2016 exhibit a similar anomalous eddy transport index, u_{duct}, but have different $C_{mlo\text{-}cgo}$ responses relative to previous years (Figure 2(a)). Since the CO_2 emitted in the Northern Hemisphere and tropics is also transported into the Southern Hemisphere by the mean divergent flow associated with the Hadley circulation, particularly during boreal summer (Miyazaki et al., 2008), this is now explored in more detail. The Pacific duct transfer in boreal winter-spring, with peaks in Feb-Apr, occurs when the CO_2 IH partial pressure difference is near maximum due to forest respiration. Likewise the mean IH transport related to the Hadley circulation occurs in boreal summer-autumn, with peaks in Jun-Aug, when the CO_2 IH partial pressure difference has a proportionally larger contribution due to the accumulated fossil fuel CO_2 from NH industrial emissions.

Figure 5 shows latitude-height cross sections, over the Pacific, averaged between 120°E-240°E, of June to August vertical wind in pressure coordinates, ω, ~~in the top panels and~~ while Figure 6 shows the corresponding results for the meridional wind, v~~, in the bottom panels~~. Recall that negative ω corresponds to positive vertical velocity in height coordinates and negative v is north-to-south meridional wind. In the boreal summer-spring average values for 1979 to 2016 show the uplift (negative ω) at low northern latitudes (Figure 5(a)) while the advective Hadley Cell meridional transfer (negative v) to the Southern Hemisphere at high altitude can be seen in Figure ~~5d~~6(a).

By subtracting the 1979-2016 average from the 2016 ω values and v values, the nature of the extreme 2016 anomaly becomes visible, with strong uplift including between 10°N and 15°N shown in Figures 5(b) and extensive meridional wind penetration into the Southern Hemisphere, particularly between 500hPa and 300hPa, shown in Figure ~~5e~~6(b).

Figures 5(c) and 6(c)~~The panels on the right~~ depict the difference between the anomaly years 2016 and 2010~~ in Figures 5c and 5f~~. Both the uplift between 10°N and 15°N and penetration of the meridional wind into the Southern Hemisphere is stronger in the upper troposphere and mean transport through convection and advection into the Southern Hemisphere more extensive in 2016.

On the basis of these figures, and similar figures for the corresponding zonally averaged quantities, we have chosen four indices to characterize the mean circulation by the Hadley Cell (Table 1). These are ω_P the vertical velocity in pressure coordinates over the Pacific ocean at 300 hPa averaged between 120°E-240°E and 10°N-15°N, v_P the meridional wind at 200hPa averaged between 120°E-240°E and 5°N-10°N as well as the corresponding zonally averaged indices ω_H and v_H introduced in Section 2.

5 Quantifying the $C_{mlo\text{-}gco}$ relationships with eddy and mean transport indices

The timing of a majority of short term variations in the 25-year baseline $C_{mlo\text{-}cgo}$ corresponds to atmospheric transport changes that influence the interhemispheric exchange. To quantify relationships between $C_{mlo\text{-}cgo}$ and the eddy and mean transport indices involved we first suppress the $C_{mlo\text{-}cgo}$ changes expected from reported anthropogenic emissions. The global annual average anthropogenic emissions (Le Quere et al., 2017) are converted to ppm using the coefficient 0.36 ppm/PgCyr^{-1} derived in Section 2 from Figure 2 and subtracted from the observed $C_{mlo\text{-}cgo}$. In Figure 6 we compare the FF-adjusted $C_{mlo\text{-}cgo}$, which we denote $C^*_{mlo\text{-}cgo}$, for two periods when $C_{mlo\text{-}cgo}$ is positive; the first is Feb-Apr that best captures the eddy IH exchange, and the second is Jun-Aug when mean transfer related to the Hadley circulation is captured.

We focus first on the FF-adjusted $C^*_{mlo\text{-}cgo}$ plots in Figures ~~6~~7(a) and (b). The mean and year-to-year variation is very much larger in (a) compared to (b) and is also larger in (a) compared to the annual averaged values in Figure 2(a). The contrasting behaviour between the two periods after 2012 is also more marked.

To emphasize the similarities between $C^*_{mlo\text{-}cgo}$ and Pacific duct winds we plot $-u_{duct}$ in Figure ~~6~~7(a), so that easterlies are shown as positive and the more frequent westerlies as negative; the timings of peaks in both panels then correspond. When winds in the Pacific duct are easterly or near zero, FF-adjusted $C^*_{mlo\text{-}cgo}$ peak or are above average; this is now more obvious

in 2016 compared with the corresponding results for $C_{mlo\text{-}cgo}$ in Dec-May shown in Figure 2(b) and 2(c). In fact the FF-adjusted $C^{*}_{mlo\text{-}cgo}$ has very similar behaviour to the detrended $C_{mlo\text{-}cgo}$, with pattern correlations of ~~detrended~~ anomalies of $r = 0.931$, $r = 0.954$ ~~and~~ and $r = 0.981$ for Jan-Dec, Jun-Aug and Feb-Apr respectively. The similarity can also be seen by comparing the top panel of Figure 7(b) with that of Figure 8. Despite persistent agreement in timing, the magnitude of the $C_{mlo\text{-}cgo}$ response to the u_{duct} anomaly is more variable. This is reflected in the correlation between the detrended $C_{mlo\text{-}cgo}$ anomalies and the detrended u_{duct} anomalies which is $r = -0.500$ for Feb-Apr and $r = -0.228$ for Dec-May. These results confirm the preferential Pacific duct transfer in late boreal winter and early spring (Feb-Apr). They also indicate that although there is an important relationship between $C_{mlo\text{-}cgo}$ and the zonal wind in the Pacific duct, other processes detailed in Section 2, such as changes in direct advective transport by the mean winds and emissions, also play roles in year-to-year IH variations. This is also confirmed by a regression analysis of $C_{mlo\text{-}cgo}$ anomalies onto u_{duct} anomalies (not shown) where there is significant scatter about the regression line.

In particular, during 2009-2010 there were a number of complicating factors that most likely contributed. The unusually low $C_{mlo\text{-}cgo}$ in 2008, 2009 coincide with the Global Financial Crisis when global emissions dipped (and recent British Petroleum, 2018, estimates of emissions suggest an even larger 2008-2009 anomaly than in data used here). Terrestrial Net Biosphere Production south of 30°S was also anomalously low in 2009 and anomalously high in 2010 (FF16; Trudinger et al. 2016; though by amounts not sufficient to impact on the Cape Grim baseline CO_2 records). The low $C_{mlo\text{-}cgo}$ also align with near-record strong westerlies in the Pacific duct, and associated larger eddy transport, in 2008; both potentially contribute to increasing the magnitude of the subsequent CO_2 step.

In Figure ~~6~~7(b) the post-2010 decrease in Jun-Aug FF-adjusted $C^{*}_{mlo\text{-}cgo}$ is clearly ~~indicated~~ mirrored in the decreasing ω and v indices (indicating strengthened Hadley circulation) , particularly in the 120°E-240°E Pacific sector (ω_P and v_P) compared to the zonal average (ω_H and v_H). The considerably weaker strength of the Hadley circulation in 2010 compared with 2016 is shown quite distinctly. The correlations between the detrended $C_{mlo\text{-}cgo}$ anomalies and indices of mean transport are shown in Table ~~1~~2.

Generally Jun-Aug correlations are stronger than the Jun-Nov correlations and correlations over the Pacific sector 120°E-240°E are generally larger than for the zonally averaged quantities. This is clearly the case for ω while v_H is an exception being larger for the longer time period. The $C_{mlo\text{-}cgo}$ correlations for Jun-Aug involving ω_P and v_P have roughly similar magnitudes to those for Feb-Apr involving u_{duct} and ω_P and v_P provide similar predictability of the role of the Hadley circulation in mean IH CO_2 transport as u_{duct} does for eddy transport. Interestingly, during 2009-2010 the effects of u_{duct} and ω_P and v_P reinforce to make the step in $C_{mlo\text{-}cgo}$ large, while for 2015-2016 ω_P and v_P counteract u_{duct} and the exceptionally strong Hadley circulation becomes the dominant feature in determining the annual $C_{mlo\text{-}cgo}$ (Figure 1a). These results show that there is an important connection between the $C_{mlo\text{-}cgo}$ and the indices that characterize the strength of the Hadley circulation and mean transport. Again, as also suggested by regression analysis (not shown), other processes, detailed in Section 2 and above, also play important roles.

The somewhat different behaviours of $C_{mlo-cgo}$ and the dynamical indices, particularly during the El Niños of 2009-2010 and 2015-2016 and of 1997-1998, may partly reflect the diversity of El Niños and whether the heating is focussed in the Eastern Pacific or in the Central Pacific (Capotondi et al. 2015; L'Heureux et al. 2017 and references therein). The strong 1997-1998 event like, the 1982-1983 event, was a classic Eastern Pacific El Niño with maximum temperature anomalies there of nearly $+4^{o}$ C (L'Heureux et al. 2017). The 2009-2010 event in contrast was a Central Pacific El Niño with record-breaking warming in the central Pacific (Kim et al. 2011). The 2015-2016 El Niño fell between these two canonical cases with less warming in the eastern Pacific Ocean than the 1997-1998 event but similar warming to the 2009-2010 event in the central Pacific (L'Heureux et al. 2017).

The broadly increasing magnitude of the negative ω and v indices since 2012 is associated with both increasing global temperatures, breaking the record in 2016, –and the large El Niño of 2015 and 2016. This has resulted in the increasing importance of the mean convective and advective CO_2 transport by the Hadley circulation relative to the eddy transport including through the Pacific duct. It will be interesting to see whether this favouring of the mean over the eddy IH CO_2 transport will become increasingly important with further global warming and the extent to which it depends on extreme El Niños (Cai et al., 2014; Freitas et al., 2017; Yeh et al., 2018).

The dynamical indices that we have used for this study are based on the NCEP-NCAR reanalysis (NNR) data (Kalnay et al. 1996). There is generally close correspondence between the major global atmospheric circulation data sets that, like the NNR data, use full data assimilation throughout the atmosphere (Frederiksen & Frederiksen 2007; Frederiksen et al. 2017; Rikus 2018). We have confirmed this by recalculating our dynamical indices and main correlations with $C_{mlo-cgo}$ based on the NASA Modern Era Retrospective-analysis for Research and Applications (MERRA) data (Rienecker et al. 2011). For example, the 1992 to 2016 correlation between MERRA and NNR data for u_{duct} in Feb-Apr is $r = 0.974$, for ω_P in Jun-Aug is $r = 0.899$ and for v_P in Jun-Aug is $r = 0.931$. The corresponding correlations between detrended anomalies of $C_{mlo-cgo}$ and the MERRA based dynamical indices are also very similar. The correlations are $r = -0.512$ with u_{duct} for Feb-Apr (compared with $r = -0.500$ for the NNR index), $r = 0.504$ with ω_P for Jun-Aug (compared with $r = 0.522$ based on NNR) and $r = 0.538$ with v_P for Jun-Aug (compared with $r = 0.539$ based on NNR).

6 Interhemispheric exchange of other trace gases

Next, we consider the eddy and mean IH exchange of other trace gas species and their correlations with CO_2 and dynamical indices of transport. We focus on Feb-Apr for eddy transport and Jun-Aug for mean transport since these periods were the peaks for correlations of CO_2 IH difference with eddy and mean transport indices respectively. However, there are differences in the seasonal variability of interhemispheric gradient in the different trace gas species that are reflected in their transport and for that reason we also briefly mention the results for other time periods. We begin by further examining Mauna Loa minus Cape Grim (mlo–cgo) differences, between 1992-2016, in the routinely monitored CSIRO species CH_4, CO and H_2 in addition to CO_2 that were briefly considered in Frederiksen and Francey (FF16), as well as N_2O (for 1993-

2016). Thereafter we discuss mlo–cgo differences in SF_6 data sourced from the NOAA Halocarbons and other Atmospheric Trace Species Group (HATS) program from 1998 (NOAA, 2018).

6.1 Pacific westerly duct and eddy IH transport of CSIRO monitored trace gases

The IH exchange of the trace gas species, CH_4, CO and H_2, in addition to CO_2, and the role of the Pacific westerly wind duct were also considered in FF16. In particular, the covariance, of the mlo–cgo difference in these routinely monitored CSIRO species with u_{duct}, is shown in Figure 5 of FF16. We recall that the u_{duct} index is the average zonal wind in the region 5°N to 5°S, 140°W to 170°W at 300hPa. As noted in FF16, the extreme cases of Pacific westerly duct closure in 1997–98 and 2009–10 show up in the reduction of seasonal IH exchange for CH_4 and CO as well as CO_2. The similar behaviour of detrended anomalies of mlo–cgo difference in CH_4, CO and CO_2 and their correlations with u_{duct} is shown in Table 3 for Feb–Apr. We note the quite high correlations of CH_4 and CO with CO_2 ($r = 0.697$ and $r = 0.645$ respectively) and the significant anti–correlations of all these three species with u_{duct} ($r = -0.448$, $r = -0.605$ and $r = -0.500$ respectively). In fact, for Mar-May the correlation between CH_4 and CO_2 is even larger at $r = 0.728$ (and with u_{duct} it is $r = -0.474$) while between CO and CO_2 it is $r = 0.611$ (and with u_{duct} it is $r = -0.507$). These results are of course consistent with Figure 5 of FF16 and are further evidence of similarities of IH transient eddy transport of these three gases. Table 3 also shows that the Feb-Apr correlation of H_2 with CO_2 and anti–correlation with u_{duct} have smaller magnitudes ($r = 0.296$ and $r = -0.218$ respectively). These results for anomalies are probably related to corresponding similarities and differences in the seasonal mean values (not shown) of these gases in Feb–Apr, as discussed below.

Anomalies in mlo–cgo differences in CSIRO monitored N_2O are generally poorly correlated with those in CO_2 as shown for Feb-Apr and Jun-Aug in Tables 3 and 4 respectively (the maximum 3 month average correlation is $r = 0.274$ for Mar-May) and this is mirrored in generally poor correlation with the dynamical indices shown in Tables 3 and 4. This reflects the fact that natural exchanges with equatorial agriculture and oceans are the main sources (Ishijima et al., 2009), and the seasonal range in mlo-cgo difference is only around 0.2% of the mean N_2O level, more than 10 times less than is the case for the other species.

6.2 Hadley circulation and mean IH transport of CSIRO monitored trace gases

We examine the role of the Hadley circulation on the mean transport of trace gases focusing on the boreal summer period of Jun–Aug. Table 4 shows the correlations between the detrended anomalies of mlo–cgo difference in CH_4, CO and H_2 with CO_2 and with the dynamical indices ω_P and v_P (Table 1). We note that the largest Jun-Aug correlation is between H_2 and CO_2 ($r = 0.680$) and the correlations between CH_4 and CO with CO_2 are considerably smaller ($r = 0.246$ and $r = 0.108$ respectively) while for Apr-Jun the latter correlations are more comparable at $r = 0.583$ and $r = 0.496$ respectively. These correlations with CO_2 are also reflected in the respective correlations of the other trace gases with ω_P and v_P. We note from Table 4 that the Jun-Aug correlations of H_2 with ω_P and v_P are $r = 0.427$ and $r = 0.442$ respectively which is

slightly less than the corresponding correlations between CO_2 and the dynamical indices ($r = 0.522$ and $r = 0.539$ respectively) but considerably larger than for CH_4 and CO. For May-Jul the correlation of H_2 with ω_P is slightly larger with $r = 0.526$.

Again, the different behaviour of the trace gas anomalies may be related to their different seasonal mean values; the seasonal mean IH difference for H_2 peaks in boreal summer while for CH_4 and CO it is relatively low with a minimum in August. The distribution and variability of surface exchange is different for each of the trace gases and there is potential for this to interact with the restricted extent and seasonal meandering of the regions of uplift to influence IH exchange of a species. For example, 70% of the global total CH_4 emissions are from mainly equatorial biogenic sources that include wetlands, rice agriculture, livestock, landfills, forests, oceans and termites (Denman et al., 2007) and CO emissions contain a significant contribution from CH_4 oxidation and from tropical biomass burning.

A more detailed examination of the inter–annual variation of the mlo–cgo difference in H_2 during boreal summer is presented in Figure 8. It shows the detrended H_2 data in comparison with the corresponding CO_2 data and with the ω_P and v_P indices. First we note that the detrended CO_2 data in the top panel has very similar inter–annual variation to the FF–adjusted $C^*_{\text{mlo-cgo}}$ in Figure 7(b). We also see that the qualitative behaviour of H_2 mirrors many aspects of CO_2, as expected from the correlations in Table 4. In particular, the increase in the IH difference of H_2 in 2010 is even more pronounced than for CO_2. For CO_2 and for H_2 there is a steady reduction in the IH difference from around 2013 leading to a local minimum in 2016. In both of these respects these gases broadly follow the changes in the Hadley circulation including the strengthening during 2015–2016. Vertical lines in Figure 8 indicate other times between 1992 and 2016 when transitions occur in both these trace gases and in the Hadley circulation characterized by ω_P and v_P.

Surface exchanges of H_2 have similarities to those of CO_2 in that they occur mostly at mid–northern latitudes and are mainly due to emissions from fossil fuel combustion. However H_2 also has mid–northern latitude photochemical sources peaking in August (Price et al., 2007). These boreal summer sources are almost offset by a combined soil and hydroxyl sink, but the overall interhemispheric partial pressure difference is boosted by a significant reduction in the Southern Hemisphere photochemical source at that time. For both species, the most northern excursions of the inter–tropical convergence zone that occurs at Pacific latitudes encounter increasing concentrations of both gases.

As noted above, anomalies in mlo–cgo differences in N_2O are poorly correlated with those in CO_2 and in dynamical indices (Tables 3 and 4). Indeed the 3 month average anti-correlation with u_{duct} that has the largest magnitude is $r = -0.133$ for Mar-May and the largest correlations with ω_P is $r = 0.359$ for Apr-Jun and with v_P is $r = 0.350$ for May-Jul.

6.3 Interhemispheric exchange of SF_6

In the case of SF6 we have analysed the mlo–cgo difference in available NOAA HATS data from 1998 to 2012 when cgo HATS measurements ceased. Correlations (Tables 3 and 4) of detrended anomalies in IH differences in SF_6 with those in CO_2 are as follows: the Feb–Apr correlation is $r = 0.619$, the Mar-May correlation is $r = 0.722$, the Apr-Jun correlation is $r = 0.595$, the May–Jul correlation is $r = 0.303$ and the Jun–Aug correlation is $r = 0.223$. The corresponding

correlations with dynamical indices are as follows: for Feb–Apr the correlation with u_{duct} is $r = -0.617$, the May–Jul correlations with ω_P is $r = 0.465$, the Jun–Aug correlation with ω_P is $r = 0.433$, the May–Jul correlation with v_P is $r = 0.517$ and the Jun–Aug correlation with v_P is $r = 0.385$. We note that SF_6 has an anti-correlation with u_{duct} for Feb-Apr that has larger magnitude than for CO_2 and even CO. Thus, there is again a significant influence of the Pacific westerly duct, in late boreal winter and spring, and of the Hadley circulation, in boreal summer and late spring, as measured by these indices, on the mlo–cgo differences of SF_6; these SF_6 differences exhibit a similar step change in 2009-2010 as shown for CO_2 in Figures 2 and 7.

~~6~~7 Conclusions

The major El Niño of 2015 and 2016 coincided with record global warming, with 2016 having the highest global average surface temperatures and 2015 the third highest (2017 had the second highest). The strength of the Hadley circulation also increased to unprecedented levels during 2015-2016 and had a major impact on the mean interhemispheric (IH) transport of CO_2 and on the difference in CO_2 concentration between Mauna Loa and Cape Grim ($C_{mlo\text{-}cgo}$). This study has focussed on the roles of IH transient eddy and mean transport of CO_2 on interannual variations in $C_{mlo\text{-}cgo}$ and has established dynamical indices that characterize the broad features of this transfer (Table 1). Interestingly, some of these indices are based on regions that lie close to or overlap the region of the Niño 3.4 SST index (5°N-5°S, 120°W-170°W) where ENSO is strongly coupled to the overlying atmosphere (L'Heureux et al., 2017).

One of these indices, u_{duct}, which is a measure of eddy IH transport of CO_2, was introduced in FF16. This index is the 300 hPa Pacific zonal wind averaged between 5°N-5°S and 140°W-170°W and is strongly correlated with the Southern Oscillation (SOI) index ($r \sim 0.8$ in Figure 4(a) of FF16). A particular focus of that study was to propose an explanation for the record step in CO_2 IH difference between 2009 and 2010 and it was concluded that the closing of the Pacific duct (negative u_{duct}) during the El Niño of 2010 was a significant contributing factor. It was also noted that there were half a dozen other occasions going back to the 1960s when the closing of the Pacific duct was related to an increase in CO_2 IH difference (Keeling et al., 2009).

Here, we have extended the analysis of the relationship between u_{duct} and $C_{mlo\text{-}cgo}$ to 2016. We again find that during boreal winter-spring, and particularly during Feb-Apr when eddy transport of CO_2 from the Northern to Southern Hemispheres is most active, there is an increase in $C_{mlo\text{-}cgo}$ during the El Niño of 2015-2016. However, while the timing of the increases in these years, and for other occasions going back to 1992, agree with the closing of the Pacific duct the magnitude is more variable indicating the contribution of other processes discussed in Section 2. We have analysed the intermittent nature of the opening and closing of the Pacific westerly duct. In particular, episodes in February 2015 have been related to results from NASA (2016) data in the movie 'Following Carbon Dioxide through the Atmosphere'. The movie provides further evidence of the propagation of Rossby waves through the open Pacific westerly duct and the transfer of CO_2 into the

Southern Hemisphere. We have also noted that large scale uplift slightly downstream of Asia occurs when the Pacific duct is open allowing these substantial emissions to be transported directly, via Rossby wave dispersion, through the duct.

A major focus of this article has also been the role of changes in the mean IH CO_2 transport from the Northern to Southern Hemispheres due to variability in the Hadley circulation. We have introduced indices (Table 1) that measure this transfer based on the 300 hPa ω, the vertical velocity in pressure coordinates, between 10°N and 15°N and 200 hPa v, the meridional wind between 5°N and 10°N, both zonally averaged (ω_H and v_H) and with averaging restricted to the Pacific sector 120°E-240°E (ω_P and v_P). The correlations for Jun-Aug between $C_{mlo\text{-}cgo}$ and ω_P or v_P ($r \sim 0.5$) have roughly similar magnitudes to those in Feb-Apr involving u_{duct}. The indices ω_P and v_P provide similar predictability of the role of the Hadley circulation in mean IH CO_2 transport as u_{duct} does for eddy transport. We have also found that, during 2009-2010 the effects of u_{duct} and ω_P and v_P reinforce to make the step in $C_{mlo\text{-}cgo}$ large. In contrast, for 2015-2016 ω_P and v_P counteract u_{duct} and the record Hadley circulation primarily determines the annual Mauna Loa and Cape Grim CO_2 difference. The effects of interannual changes in mean and eddy transport on IH gradients in CO_2 (and CH_4, CO, H_2, N_2O and SF_6) has been examined for the period 1992 to 2016.

The sign and strength of zonal winds in the Pacific westerly duct (u_{duct}) are related to Rossby wave dispersion and breaking and are correlated with corresponding changes in near-equatorial transient kinetic energy (Fig. 6, Frederiksen and Webster 1988) resulting in intermittent changes in the mixing of trace gases. This effect may not be adequately represented in the parameterizations (Frederiksen et al. 2016) used in atmospheric circulation and transport models. Model determinations of short term variations in the Hadley circulation exchange are also susceptible to uncertainties in representations of the equatorial convective dynamics (Lintner et al. 2004). Over at least 25 years, much of the variability in CO_2 between the two surface monitoring sites of Mauna Loa and Cape Grim can be associated with dynamical near-equatorial atmospheric indices of global significance in a changing climate. The changing nature of the seasonal and inter annual changes in CO_2 IH Pacific duct eddy and mean Hadley circulation transfer between 1992 through to 2016 provides an interesting case study and potential test of inversion models of atmospheric transport.

We plan to further explore trace gas IH transfer focussing on Southern Hemisphere CO_2 stable isotope data in a study that distinguishes between mean IH transfer and eddy transfers of both current season emissions and accumulated Northern Hemisphere fossil fuel emissions.

Data availability. Meteorological data is available from the NOAA/ESRL web site: http://www.esrl.noaa.gov/psd/ and from the NASA web site: https://giovanni.gsfc.nasa.gov/giovanni/ and ~~CO2~~ trace gas data is available upon request from the corresponding author (jorgen.frederiksen@csiro.au).

Author contributions. J. S. Frederiksen provided information on atmospheric dynamics and the roles of transport mechanisms and R. J. Francey provided the ~~CO_2~~ trace gas information. Both contributed to the writing of the paper.

Competing interests. The authors declare that they have no conflicts of interest.

Acknowledgements. We thank Nada Derek and Stacey Osbrough for assistance with the graphics and Paul Steele has provided valuable advice on the manuscript. The sustained focus and innovation of CSIRO GASLAB personnel, and skilled trace gas sample collection by personnel at the Bureau of Meteorology Cape Grim Baseline Atmospheric Program and NOAA's Mauna Loa stations underpin the progress reported here. ~~Paul Steele has provided valuable advice on the manuscript.~~ The dynamics contributions were prepared using data and software from the NOAA/ESRL Physical Sciences Division web site: http://www.esrl.noaa.gov/psd/ except, as stated in Section 6, where NASA MERRA data was also used from the web site: https://giovanni.gsfc.nasa.gov/giovanni/. We acknowledge NASA Goddard Flight Center and their Production Team for the movie 'Following Carbon Dioxide through the Atmosphere' available at the web site: https://svs.gsfc.nasa.gov/12445. The trace gas data for CSIRO monitored species CO_2, CH_4, CO, H_2 and N_2O and the NOAA monitored SF_6 are available from the World Data Centre for Greenhouse Gases website: https://ds.data.jma.go.jp/gmd/wdcgg/cgi-bin/wdcgg/catalogue.cgi.

References

1. Andres, R. J., Boden, T. A., ~~and~~ & Higdon D.: A new evaluation of the uncertainty associated with CDIAC estimates of fossil fuel carbon dioxide emission, Tellus B 66, 23616, 2014.
2. Bowman, K. P., &~~and~~ Cohen, P. J.: Interhemispheric exchange by seasonal modulation of the Hadley circulation, J. Atmos. Sci., 54, 2045-2059, 1997.
3. British Petroleum: CO_2 emissions, 2018. https://www.bp.com/en/global/corporate/energy-economics/statistical-review-of-world-energy/co2-emissions.html
4. Cai, W., Borlace, S., Lengaigne, M., van Rensch, P., Collins, M., Vecchi, G., Timmermann, A., Santoso, A., McPhaden, M. J., Wu, L., England, M. H., Wang, G., Guilyardi, E., &~~and~~ Jin, F. F. : Increasing frequency of extreme El Niño events due to greenhouse warming, Nature Climate Change, 4, 111-116, doi:10.1038/nclimate2100, 2014.
5. ~~4.~~ Capotondi, A., Wittenberg, T., Newman, M., Lorenzo, E. D., Yu, J. Y., Braconnot, P., Cole, J., Dewitte, B., Giese, B., Guilyardi, E., Jin, F. F., Karnauskas, K., Kirtman, B., Lee, T., Schneider, N., Xue, Y., & Yeh, S. W.: Understanding ENSO diversity, Bull. Amer. Meteor. Soc., 96, 921–938, doi: 10.1175/BAMS-D-13-00117.1, 2015.
6. ~~5.~~ Chatterjee, A., Gierach, M. M., Sutton, A. J., Feely, R. A., Crisp, D., Eldering, A., Gunson, M. R., O'Dell, C. W., Stephens, B. B., &~~and~~ Schimel, D. S.: Influence of El Niño on atmospheric CO2 over the tropical Pacific Ocean: Findings from NASA's OCO-2 mission, Science, 358, eaam5776, doi:10.1126/science.aam5776, 2017.
7. ~~Ciais, Ph., Reichstein, M., Viovy, N., Granier, A., Ogée, J., Allard, V., Aubinet, M., Buchmann, N., Bernhofer, Chr., Carrara, A., Chevallier, F., De Noblet, N., Friend, A. D., Friedlingstein, P., Grünwald, T., Heinesch, B., Keronen, P.,~~

~~Knohl, A., Krinner, G., Loustau, D., Manca, G., Matteucci, G., Miglietta, F., Ourcival, J. M., Papale, D., Pilegaard, K., Rambal, S., Seufert, G., Soussana, J. F., Sanz, M. J., Schulze, E. D., Vesala, T., and Valentini, R.: Europe-wide reduction in primary productivity caused by the heat and drought in 2003, Nature, 437, 529–533, 2005.~~Denman, K. L., Brasseur, G., Chidthaisong, A., Ciais, P., Cox, P. M., Dickinson, R. E., Hauglustaine, D., Heinze, C., Holland, E., Jacob, D., Lohmann, U., Ramachandran, S., da Silva Dias, P. L., Wofsy, S. C., & Zhang, X.: Couplings Between Changes in the Climate System and Biogeochemistry. In: *Climate Change 2007: The Physical Science Basis. Contribution of Working Group I to the Fourth Assessment Report of the Intergovernmental Panel on Climate Change* [Solomon, S., Qin, D., Manning, M., Chen, Z., Marquis, M., Averyt, K.B., Tignor, M. & Miller, H.L. (Eds.)]. Cambridge University Press, Cambridge, United Kingdom and New York, NY, USA, 2007.

8. Dlugokencky, E. J., Lang, P.M., Masarie, K.A., Crotwell, A.M., and Crotwell, M.J.: Atmospheric Carbon Dioxide Dry Air Mole Fractions from the NOAA ESRL Carbon Cycle Cooperative Global Air Sampling Network, 1968-2013, Version: 2014-06-27, 2014. Path: ftp://aftp.cmdl.noaa.gov/data/trace_gases/co2/flask/surface/

9. Francey, R. J., & Frederiksen, J. S.: Response to Poulter (Biogeosciences Discuss., 12, C7009-C7011, 2015), Biogeosciences Discuss., 12, C7771, Supplement, 2015. http://www.biogeosciences-discuss.net/12/C7771/2015/bgd-12-C7771-2015-supplement.pdf

~~6.~~

~~7.~~10. Francey, R. J.,~~ and~~ & Frederiksen, J. S.: The 2009–2010 step in atmospheric CO_2 interhemispheric difference, Biogeosciences, 13, 873- 885, doi: 10.5194/bg-13-873-2016, 2016.

11. Freitas, A. C. V., Frederiksen, J. S., O'Kane, T. J., &~~and~~ Ambrizzi, T.: Simulated austral winter response of the Hadley circulation and stationary Rossby wave propagation to a warming climate, Clim. Dyn., 49, 521–545, doi: 10.1007/s00382-016-3356-4, 2017.

12. Frederiksen, C. S., Frederiksen, J. S., Sisson, J. M., & Osbrough, S. L.: Trends and projections of Southern Hemisphere baroclinicity: The role of external forcing and impact on Australian rainfall, Clim. Dyn., 48, 3261–3282, doi: 10.1007/s00382-016-3263-8, 2017.

13. Frederiksen, J. S., & Frederiksen, C. S.: Interdecadal changes in Southern Hemisphere winter storm track modes, Tellus, 59 A, 599-617, 2007.

~~8.~~14. Frederiksen, J. S., Kitsios, V., O'Kane, T. J., & Zidikheri, M. J.: Stochastic subgrid modelling for geophysical and three-dimensional turbulence. In: *Nonlinear and Stochastic Climate Dynamics*, Chapter 9, 241–275, Franzke, C. J. E., & O'Kane, T. J. (Eds.), Cambridge University Press, 2016.

15. Frederiksen, J. S. & Webster, P. J.: Alternative theories of atmospheric teleconnections and low-frequency fluctuations, Rev. Geophys., 26, 459-494, 1988.

~~9.~~16. Ishijima, K., Nakazawa, T., & Aoki, S.: Variations of atmospheric nitrous oxide concentration in the northern and western Pacific, Tellus B, 61:2, 408–415, doi: 10.1111/j.1600-0889.2008.00406.x, 2009.

~~10.~~17. Kalnay, E., Kanamitsu, M., Kistler, R., Collins, W., Deaven, D., Gandin, L., Iredell, M., Saha, S., White, G., Woollen, J., Zhu, Y., Leetmaa, A., Reynolds, R., Chelliah, M., Ebisuzaki, W., Higgins, W., Janowiak, J., Mo, K. C., Ropelewski, C., Wang, J., Jenne, R., &~~and~~ Joseph, D.: The NCEP/NCAR Reanalysis 40-year Project, Bull. Amer. Meteor. Soc., 77, 437-471, 1996.

18. Keeling, R. F., Piper, S. C., Bollenbacher, A. F., and Walker, J. S.: Atmospheric CO_2 records from sites in the SIO air sampling network, In Trends: A Compendium of Data on Global Change. Carbon Dioxide Information Analysis Center, Oak Ridge National Laboratory, U.S. Department of Energy, Oak Ridge, Tenn., USA, 2009.

19. Keenan, T. F., Prentice, I. C., Canadell, J. G., Williams, C. A., Wang, H., Raupach, M. & Collatz, G. J.: Recent pause in the growth rate of atmospheric CO_2 due to enhanced terrestrial carbon uptake, Nature Communications, doi: 10.1038/ncomms13428, 2016.

~~11.~~20. Kim, W. M., Yeh, S. W., Kim, J. H., Kug, J. S., & Kwon, M. H.: The unique 2009–2010 El Niño event: A fast phase transition of warm pool El Niño to La Niña, Geophys. Res. Lett., 38, L15809, doi: 10.1029/2011GL048521, 2011.

~~12.~~21. Krol, M., de Bruine, M., Killaars, L., Ouwersloot, H., Pozzer, A., Yin, Y., Frederic Chevallier, F., Bousquet, P., Patra, P., Belikov, D., Maksyutov, S., Dhomse, S., Wuhu Feng, W., &~~and Martyn P.~~ Chipperfield, M. P.~~-~~: Age of air as a diagnostic for transport time-scales in global models. Geosci. Model Dev. Discuss., doi: 10.5194/gmd-2017-262, 1–33, 2017.

~~13.~~22. Le Quéré, C., Andrew, R. M., Friedlingstein, P., Sitch, S., Pongratz, J., Manning, A. C., Korsbakken, J. I., Peters, G. P., Canadell, J. G., Jackson, R. B., Boden, T. A., Tans, P. P., Andrews, O. D., Arora, V. K., Bakker, D. C. E., Barbero, L., Becker, M., Betts, R. A., Bopp, L., Chevallier, F., Chini, L. P., Ciais, P., Cosca, C. E., Cross, J., Currie, K., Gasser, T., Harris, I., Hauck, J., Haverd, V., Houghton, R. A., Hunt, C. W., Hurtt, G., Ilyina, T., Jain, A. K., Kato, E., Kautz, M., Keeling, R. F., Klein Goldewijk, K., Körtzinger, A., Landschützer, P., Lefèvre, N., Lenton, A., Lienert, S., Lima, I., Lombardozzi, D., Metzl, N., Millero, F., Monteiro, P. M. S., Munro, D. R., Nabel, J. E. M. S., Nakaoka, S.-I., Nojiri, Y., Padín, X. A., Peregon, A., Pfeil, B., Pierrot, D., Poulter, B., Rehder, G., Reimer, J., Rödenbeck, C., Schwinger, J., Séférian, R., Skjelvan, I., Stocker, B. D., Tian, H., Tilbrook, B., van der Laan-Luijkx, I. T., van der Werf, G. R., van Heuven, S., Viovy, N., Vuichard, N., Walker, A. P., Watson, A. J., Wiltshire, A. J., Zaehle, S., &~~and~~ Zhu, D.: Global carbon budget 2017, Earth Syst. Sci. Data Discuss., 1–79, doi:10.5194/essd-2017-123, 2017. ~~(In review).~~

~~14.~~23. L'Heureux, M. L.,Takahashi, K., Watkins, A. B., Barnston, A. G., Becker, E. J., Liberto, T. E., Gamble, F., Gottschalck, J., Halpert, M. S., Huang, B., Mosquera-Vásquez, K., &~~and~~ Wittenberg, A. T. : Observing and predicting the 2015/16 El Niño, Bull. Amer. Met. Soc., 98, 1363–~~-~~1382, doi:10.1175/BAMS-D-16-0009.1, 2017.

~~15.~~24. Lintner, B. R., Gilliand, A. B., &~~and~~ Fung, I. Y.: Mechanisms of convection-induced modulation of passive tracer interhemispheric transport annual variability, J. Geophys. Res., 109, D13102, doi: 10.1029/2003JD004306, 2004.

~~16.~~25. Miyazaki, K., Patra, P. K., Takigawa, M., Iwasaki, T. &~~and~~ Nakazawa T.: Global-scale transport of carbon dioxide in the troposphere, J. Geophys. Res., 113, D15301, doi: 10.1029/2007JD009557, 2008.

~~17.~~26. NASA: Following carbon dioxide through the atmosphere, 2016. https://svs.gsfc.nasa.gov/12445

https://www.nasa.gov/feature/goddard/2016/eye-popping-view-of-co2-critical-step-for-carbon-cycle-science

27. Ortega, S., Webster, P. J., Toma, V., & Chang, H. R.: The effect of potential vorticity fluxes on the circulation of the tropical upper troposphere, Quart. J. Roy. Met. Soc., doi: 10.1002/qj.3261, 2018.

18.28. Pandey, S., Houweling, S., Krol, M., Aben, I., Monteil, G., Nechita-Banda, N., Dlugokencky, E. J., Detmers, R., Hasekamp, O., Xu, X., Riley, W. J., Poulter, B., Zhang, Z., McDonald, K. C., James W. C. White, J. W. C., Philippe Bousquet, P., &and Röckmann, T.: Enhanced methane emissions from tropical wetlands during the 2011 La Niña, Nature Scientific Reports 7, 45759, doi: 10.1038/srep45759, 2017.

29. Poulter, B., Frank, D., Ciais, P., Myneni, R. B., Andela, N., Bi, J., Broquet, G., Canadell, J. G., Chevallier, F., Liu, Y. Y., Running, S. W., Sitch, S., &and Guido R. van der Werf, G. R.: Contribution of semi-arid ecosystems to inter-annual variability of the global carbon cycle, Nature, 509, 600–603, 2014.

19.30. Price, H., Jaegle´, L., Rice, A., Quay, P., Novelli, P. C., & Gammon, R.: Global budget of molecular hydrogen and its deuterium content: Constraints from ground station, cruise, and aircraft observations, J. Geophys. Res., 112, D22108, doi: 10.1029/2006JD008152, 2007.

31. Rayner, P. J., Law, R. M., Allison, C. E., Francey, R. J., Trudinger, C. M. & Pickett-Heaps C.: Interannual variability of the global carbon cycle (1992–2005) inferred by inversion of atmospheric CO_2 and $\delta^{13}CO_2$ measurements, Global Biogeochem. Cycles, 22, GB3008, 2008.Rienecker, M. M., Suarez, M. J., Gelaro, R., Todling, R., Bacmeister, J., Liu, E., Bosilovich, M. G., Schubert, S. D., Takacs, L., Kim, G. K., Bloom, S., Chen, J., Collins, D., Conaty, A., Da Silva, A., Gu, W., Joiner, J., Koster, R. D., Lucchesi, R., Molod, A., Owens, T., Pawson, S., Pegion, P., Redder, C. R., Reichle, R., Robertson, F. R., Ruddick, A. G., Sienkiewicz, M., & Woollen, J.: MERRA: NASA's modern-era retrospective analysis for research and applications, J. Clim. 24, 3624–3648, doi: 10.1175/JCLI-D-11-00015.1, 2011.

20.32. Rikus. L.: A simple climatology of westerly jet streams in global reanalysis datasets part 1: mid-latitude upper tropospheric jets, Clim. Dyn., 50, 2285–2310, doi: 10.1007/s00382-015-2560-y, 2018.

33. Stan, C., Straus, D.M., Frederiksen, J.S., Lin, H., Maloney, E.D. & Schumacher, C.: Review of tropical-extratropical teleconnections on intraseasonal time scales, Rev. Geophys., 55, 902-937, doi: 10.1002/2016RG000538, 2017.

34. Thoning, K. W., Tans, P. P. & Komhyr, W. D.: Atmospheric carbon dioxide at Mauna Loa Observatory, 2. Analysis of the NOAA/GMCC data, 1974 – 1985, J. Geophys. Res., 94, 8549–8565, 1989.

21.35. Trudinger, C. M., Haverd, V., Briggs, P. R., & Canadell, J. G.: Interannual variability in Australia's terrestrial carbon cycle constrained by multiple observation types, Biogeosciences, 13, 6363–6383, doi: 10.5194/bg-13-6363-2016, 2016.

22.36. Webster, P. J. & Holton, J. R.: Cross-equatorial response to mid-latitude forcing in a zonally varying basic state, J. Atmos. Sci., 39, 722–733, 1982.

37. Yeh, S. W., Cai, W., Min, S. K., McPhaden, M. J., Dommenget, D., Dewitte, B., Collins, M., Ashok, K., An, S. I., Yim, B. Y., &and Kug, J. S.: ENSO atmospheric teleconnections and their response to greenhouse gas forcing, Rev. Geophys., doi: 10.1002/2017RG000568, 2018.

~~23.~~38. Yue, C., Ciais, P., Bastos, A., Chevallier, F., Yin, Y., Rödenbeck, C., & Park, T.: Vegetation greenness and land carbon-flux anomalies associated with climate variations: a focus on the year 2015, Atmos. Chem. Phys., 17, 13903–13919, doi: 10.5194/acp-17-13903-2017, 2017.

Table captions

Table 1: Definitions of dynamical indices characterizing eddy and mean tracer transport.

Table ~~1~~2: Correlations (r) between the detrended $C_{mlo\text{-}cgo}$ anomalies and indices of mean transport ω_H, ω_P, v_H and v_P averaged for Jun-Aug and Jun-Nov 1992-2016.

Table 3: Correlations (r) between the detrended mlo–cgo gas anomalies for CO_2, CH_4, CO and H_2 with CO_2 and u_{duct} index of transient transport averaged between Feb–Apr for 1992–2016. Also shown are corresponding correlations for N_2O and 1993-2016 and for SF_6 and 1998-2012.

Table 4: Correlations (r) between the detrended mlo–cgo gas anomalies for CO_2, CH_4, CO and H_2 with CO_2 and indices of mean transport, ω_P and v_P averaged between Jun–Aug for 1992–2016. Also shown are corresponding correlations for N_2O and 1993-2016 and for SF_6 and 1998-2012.

Figure captions

Figure 1: (a) ~~Seasonal cycle of $C_{mlo\text{-}cgo}$ and u_{duct}, with area where both are positive shaded, for 1 Jan 2014 to 31 Dec 2016, (b)~~ OCO-2~~–~~ image for 17 Feb 2015 showing Rossby wave dispersion (dashed red lines) in CO_2 concentration across the equator (~~solid red~~ dotted black line); the box labeled 'OCO-2 Satellite' shows the time period of the associated movie, (b) seasonal cycle of $C_{mlo\text{-}cgo}$ and u_{duct}, with area where both are positive shaded, for 1 Jan 2014 to 31 Dec 2016, and (c) 300 hPa wind vector directions and wind strength (ms^{-1}) on 17 Feb 2015.

Figure 2: (a) Annual average $C_{mlo\text{-}cgo}$ (solid) and global CO_2 emission estimate (dashed) for 1992 to 2016, (b) $C_{mlo\text{-}cgo}$ for boreal winter-spring (blue) and summer-autumn (orange), (c) u_{duct} for boreal winter-spring (blue) and summer-autumn (orange), (d) boreal summer-autumn ω_H (orange) and v_H (green).

Figure 3: Hovmoller diagrams of 300 hPa zonal wind (ms^{-1}) averaged between 5S and 5N as a function of longitude and time for (a) 1 January 2008 to 31 December 2010, (b) 1 January 2011 to 31 December 2013 and (c) 1 January 2014 to 31 December 2016. Green through to red represent westerly winds (u -winds, ms^{-1}) over the Western~~Eastern~~ Hemisphere. White solid rounded rectangles denote the longitudinal extent of the Pacific duct and the height denotes the February to April period.

Figure 4: Correlation of vertical velocity ω (Pas^{-1}) at 300 hPa with SOI for Feb-Apr and 1948-2016.

Figure 5: Latitude height cross section of June to August 120E-240E average (a) ω (Pas^{-1}) – vertical velocity in pressure coordinates – for 1979-2016, (b) ω difference of 2016 minus 1979-2016, (c) ω difference of 2016 minus 2010~~, (d) meridional wind v (ms^{-1}) for 1979-2016, (e) meridional wind v difference of 2016 minus 1979-2016 and (f) meridional wind v difference of 2016 minus 2010~~.

Figure 6: Latitude height cross section of June to August 120E-240E average (d) meridional wind v (ms^{-1}) for 1979-2016, (e) meridional wind v difference of 2016 minus 1979-2016 and (f) meridional wind v difference of 2016 minus 2010.

Figure ~~6~~7: (a) C*$_{\text{mlo-cgo}}$ and $-u_{duct}$ averaged between Feb-Apr for 1992-2016 and (b) C*$_{\text{mlo-cgo}}$, ω_P, ω_H, v_P and v_H averaged between Jun-Aug for 1992-2016 .

Figure 8: Time series of June–August and Annual averages of detrended mlo–cgo differences in CO_2 and H_2 and June–August average dynamical indices ω_P and v_P .

Tables

~~Table 1~~

~~Time Period~~	~~ω_H~~	~~ω_P~~	~~v_H~~	~~v_P~~
~~Jun-Aug~~	~~$r = 0.361$~~	~~$r = 0.522$~~	~~$r = 0.235$~~	~~$r = 0.539$~~
~~Jun-Nov~~	~~$r = 0.297$~~	~~$r = 0.481$~~	~~$r = 0.355$~~	~~$r = 0.355$~~

Table 1: Definitions of dynamical indices characterizing eddy and mean tracer transport.

Dynamical index	Definition
u_{duct}	Average 300 hPa zonal velocity in the region 5°N to 5°S, 140°W to 170°W.
ω_H	Average 300 hPa vertical velocity in pressure coordinates in the region 10°N to 15°N, 0 to 360E.
v_P	Average 200 hPa meridional velocity in the region 5°N to 10°N, 0 to 360E.
ω_P	Average 300 hPa vertical velocity in pressure coordinates in the region 10°N to 15°N, 120E to 240E.
v_H	Average 200 hPa meridional velocity in the region 10°N to 15°N, 120E to 240E.

Table 2: Correlations (r) between the detrended $C_{mlo\text{-}cgo}$ anomalies and indices of mean transport ω_H, ω_P, v_H and v_P averaged for Jun-Aug and Jun-Nov 1992-2016.

Time Period	ω_H	ω_P	v_H	v_P
Jun-Aug	$r = 0.361$	$r = 0.522$	$r = 0.235$	$r = 0.539$
Jun-Nov	$r = 0.297$	$r = 0.481$	$r = 0.355$	$r = 0.355$

Table 3: Correlations (r) between the detrended mlo–cgo gas anomalies for CO_2, CH_4, CO and H_2 with CO_2 and u_{duct} index of transient transport averaged between Feb–Apr for 1992–2016. Also shown are corresponding correlations for N_2O and 1993-2016 and for SF_6 and 1998-2012.

Gas	CO_2	u_{duct}
CO_2	$r = 1.0$	$r = -0.500$
CH_4	$r = 0.697$	$r = -0.448$
CO	$r = 0.645$	$r = -0.605$
H_2	$r = 0.296$	$r = -0.218$
N_2O	$r = 0.215$	$r = -0.088$

SF_6	$r = 0.619$	$r = -0.617$

Table 4: Correlations (r) between the detrended mlo–cgo gas anomalies for CO_2, CH_4, CO and H_2 with CO_2 and indices of mean transport, ω_P and v_P averaged between Jun–Aug for 1992–2016. Also shown are corresponding correlations for N_2O and 1993-2016 and for SF_6 and 1998-2012.

Gas	CO_2	ω_P	v_P
CO_2	$r = 1.0$	$r = 0.522$	$r = 0.539$
CH_4	$r = 0.246$	$r = 0.195$	$r = 0.250$
CO	$r = 0.108$	$r = 0.205$	$r = 0.236$
H_2	$r = 0.680$	$r = 0.427$	$r = 0.442$
N_2O	$r = -0.010$	$r = 0.290$	$r = 0.266$
SF_6	$r = 0.223$	$r = 0.433$	$r = 0.385$

Figures-

~~Figure 1~~

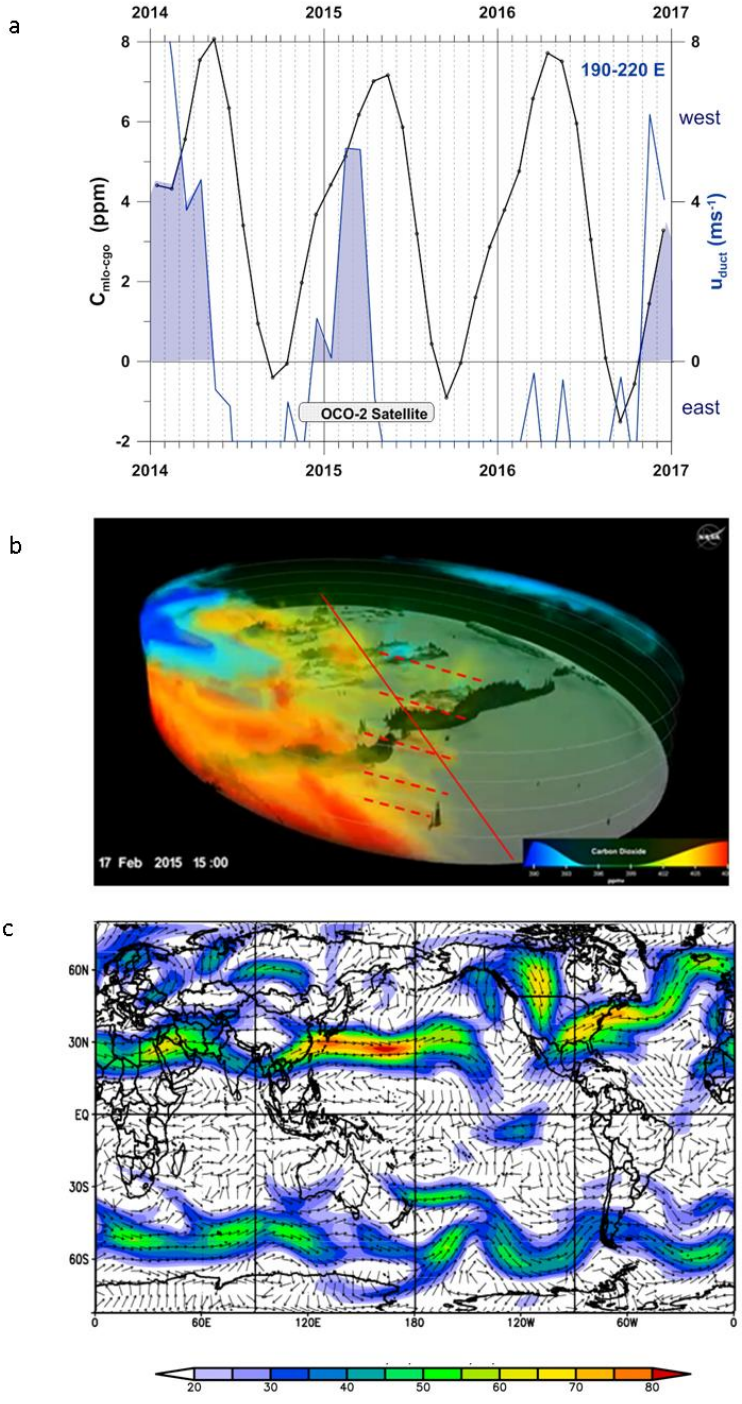
a
2014
2015
2016
2017
190-220 E
west
east
$C_{mlo-cgo}$ (ppm)
u_{duct} (ms^{-1})
OCO-2 Satellite
b
17 Feb 2015 15 :00
Carbon Dioxide
c
60N
30N
EQ
30S
60S
0
60E
120E
180
120W
60W
20
30
40
50
60
70
80

~~Figure 2~~

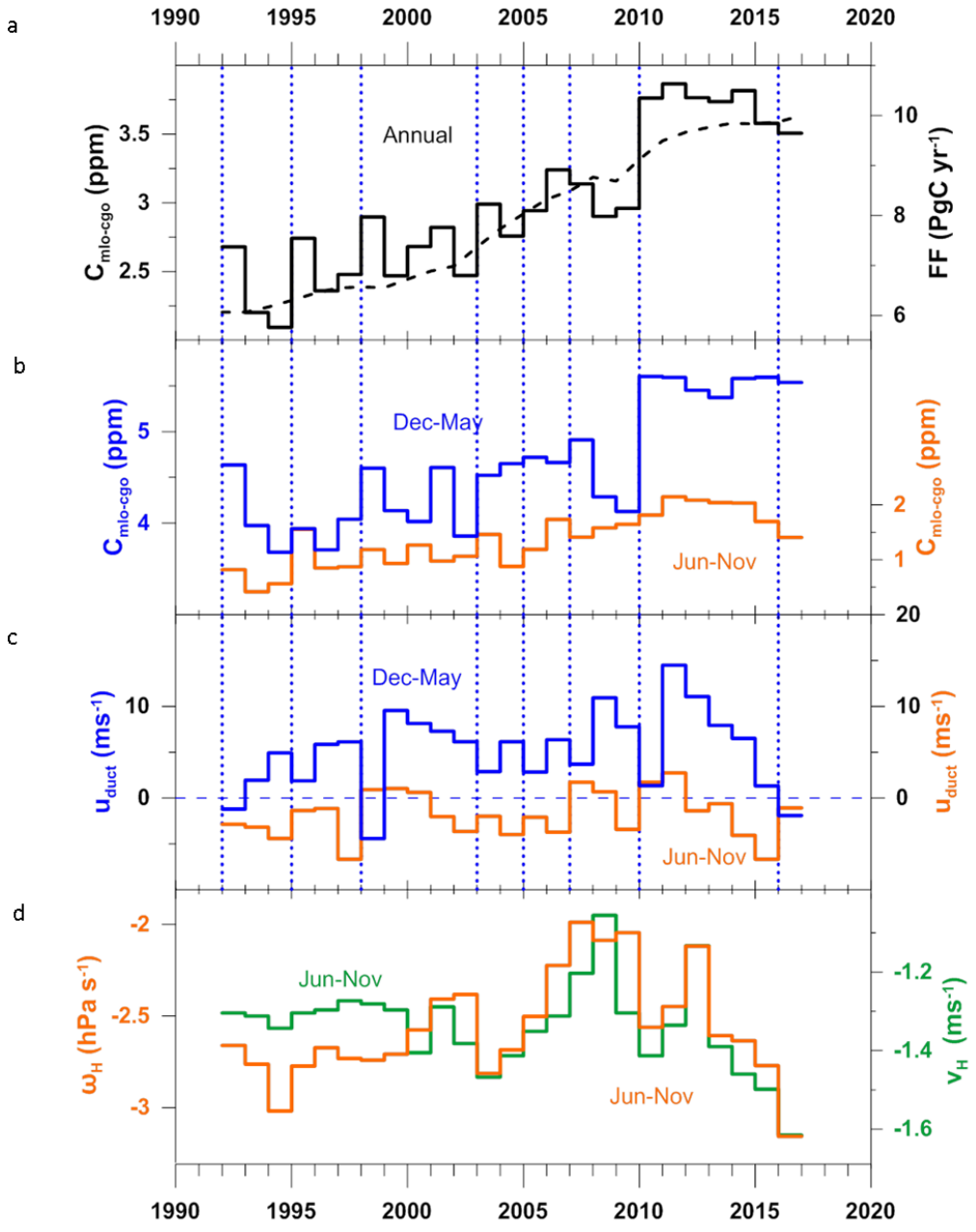
a
b
c
d
1990
1995
2000
2005
2010
2015
2020
Annual
$C_{mlo-cgo}$ (ppm)
FF (PgC yr^{-1})
Dec-May
Jun-Nov
u_{duct} (ms^{-1})
ω_H (hPa s^{-1})
v_H (ms^{-1})

~~Figure 3~~

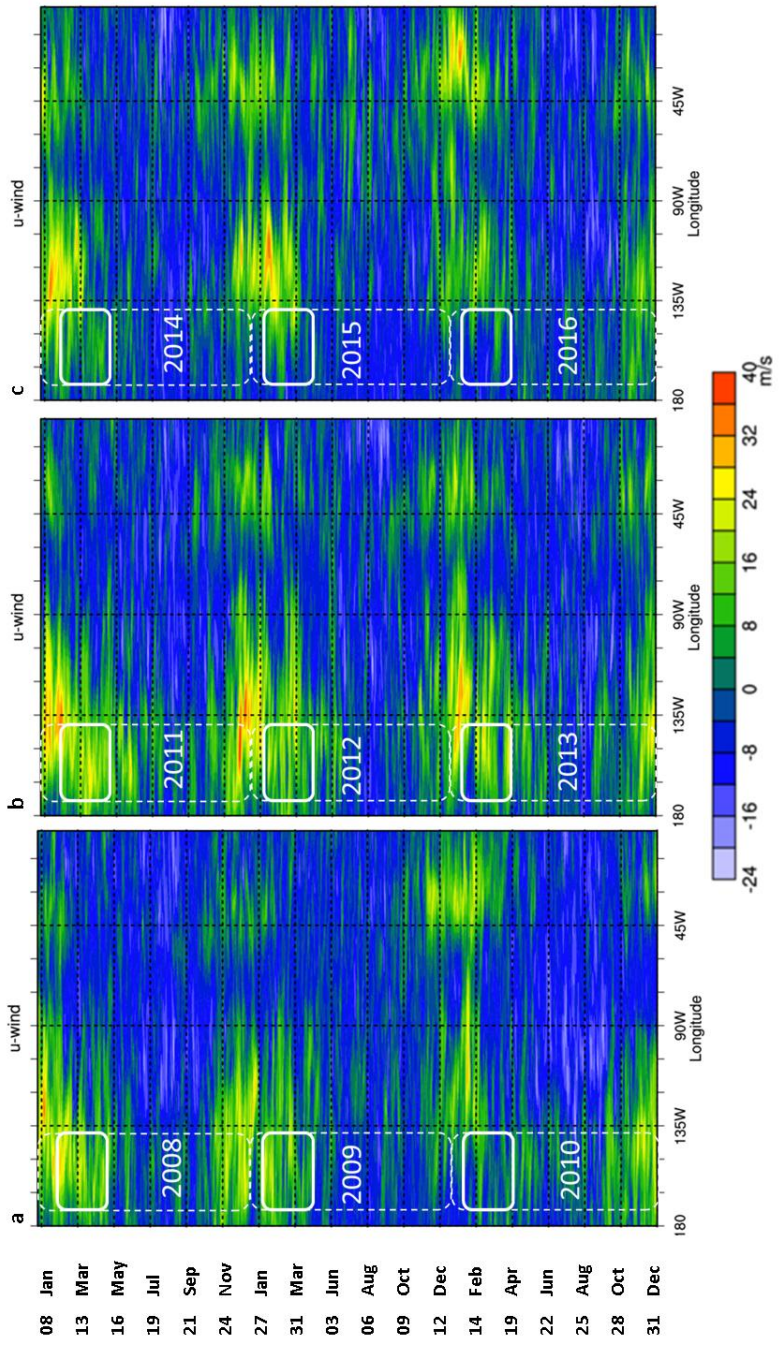
a
b
c
u-wind
Longitude
180
135W
90W
45W
2008
2009
2010
2011
2012
2013
2014
2015
2016
08 Jan
13 Mar
16 May
19 Jul
21 Sep
24 Nov
27 Jan
31 Mar
03 Jun
06 Aug
09 Oct
12 Dec
14 Feb
19 Apr
22 Jun
25 Aug
28 Oct
31 Dec
-24
-16
-8
0
8
16
24
32
40
m/s

~~Figure 4~~

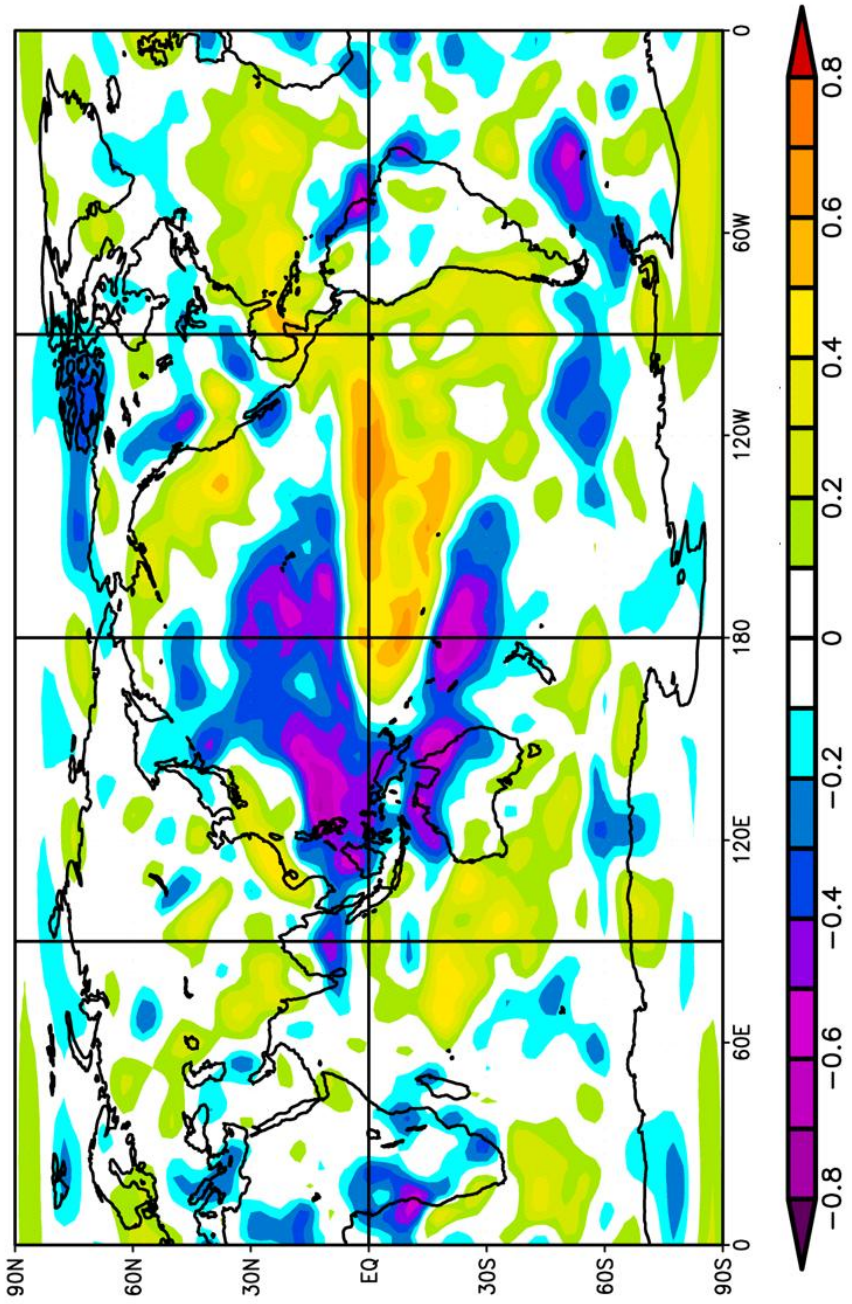
90N
60N
30N
EQ
30S
60S
90S
0
60E
120E
180
120W
60W
0
0.8
0.6
0.4
0.2
0
−0.2
−0.4
−0.6
−0.8

~~Figure 5~~

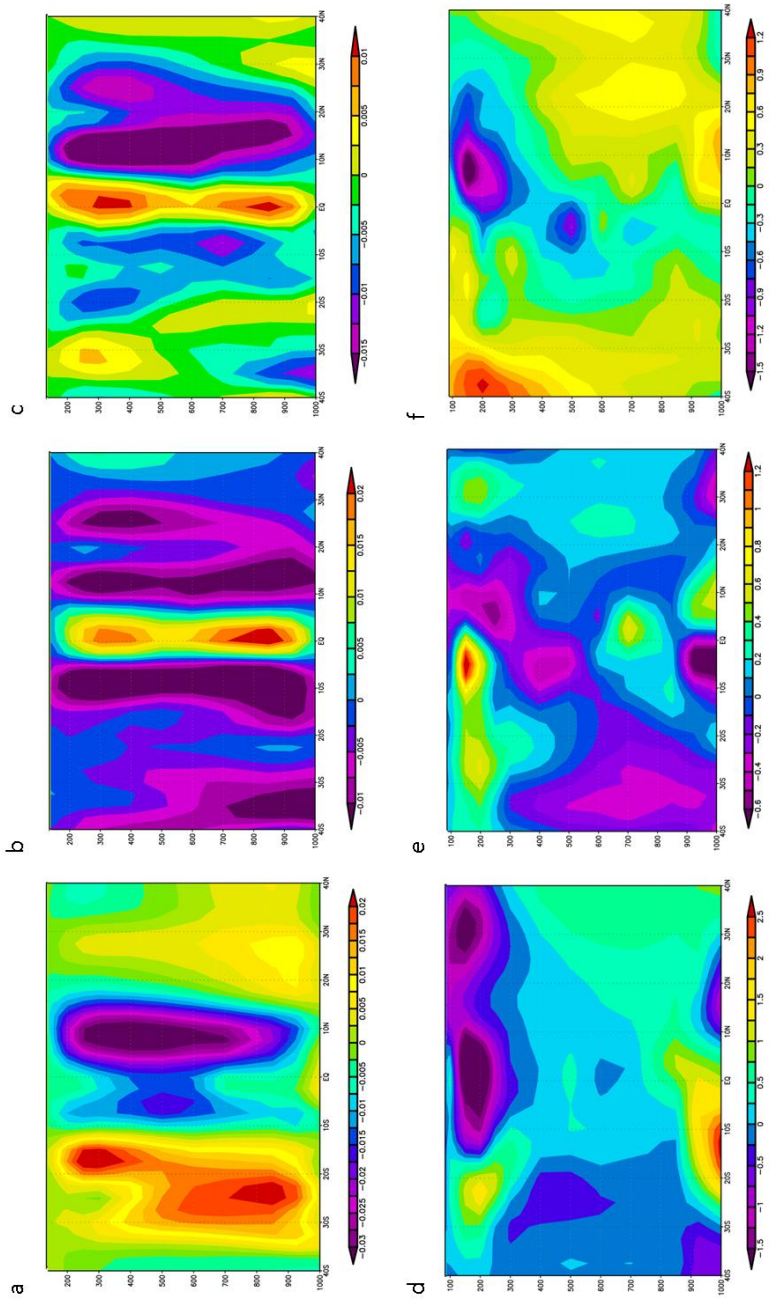

~~Figure 6~~

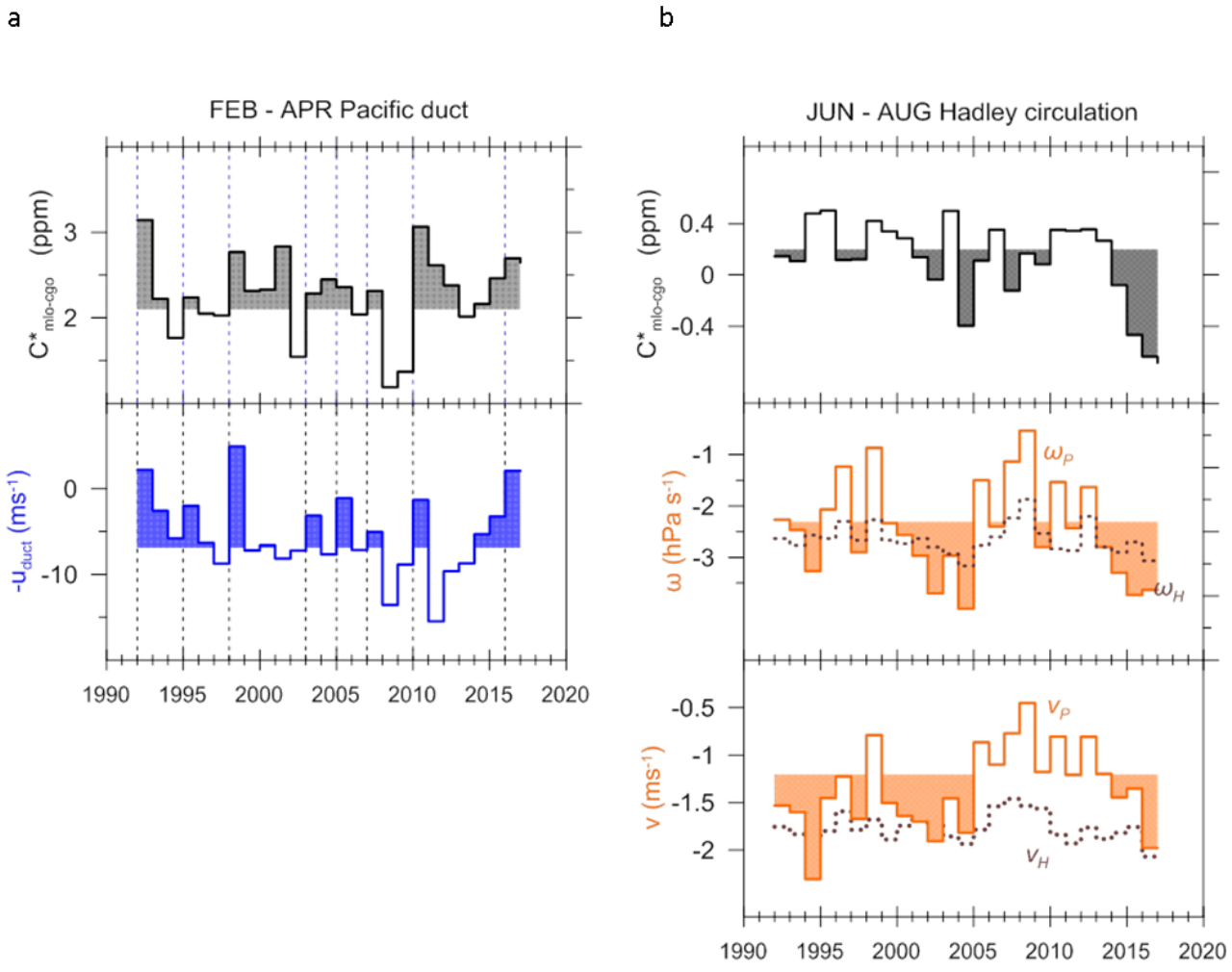
a
FEB - APR Pacific duct
C*mlo-cgo (ppm)
3
2
-uduct (ms-1)
0
-10
1990
1995
2000
2005
2010
2015
2020
b
JUN - AUG Hadley circulation
C*mlo-cgo (ppm)
0.4
0
-0.4
ω (hPa s-1)
-1
-2
-3
ωP
ωH
v (ms-1)
-0.5
-1
-1.5
-2
vP
vH
1990
1995
2000
2005
2010
2015
2020

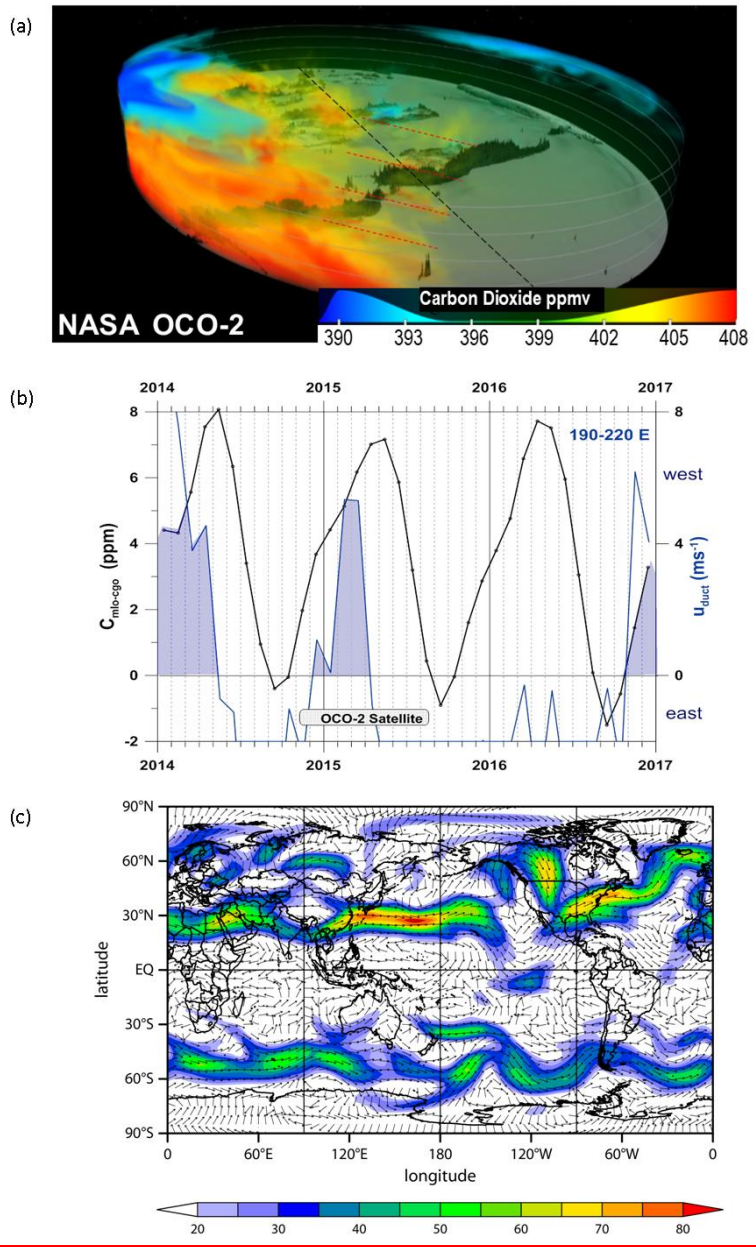

Figure 1: (a) OCO-2 image for 17 Feb 2015 showing Rossby wave dispersion (dashed red lines) in CO_2 concentration across the equator (dotted black line); the box labeled 'OCO-2 Satellite' shows the time period of the associated movie , (b) seasonal cycle of $C_{mlo-cgo}$ and u_{duct}, with area where both are positive shaded, for 1 Jan 2014 to 31 Dec 2016, and (c) 300 hPa wind vector directions and wind strength (ms^{-1}) on 17 Feb 2015.

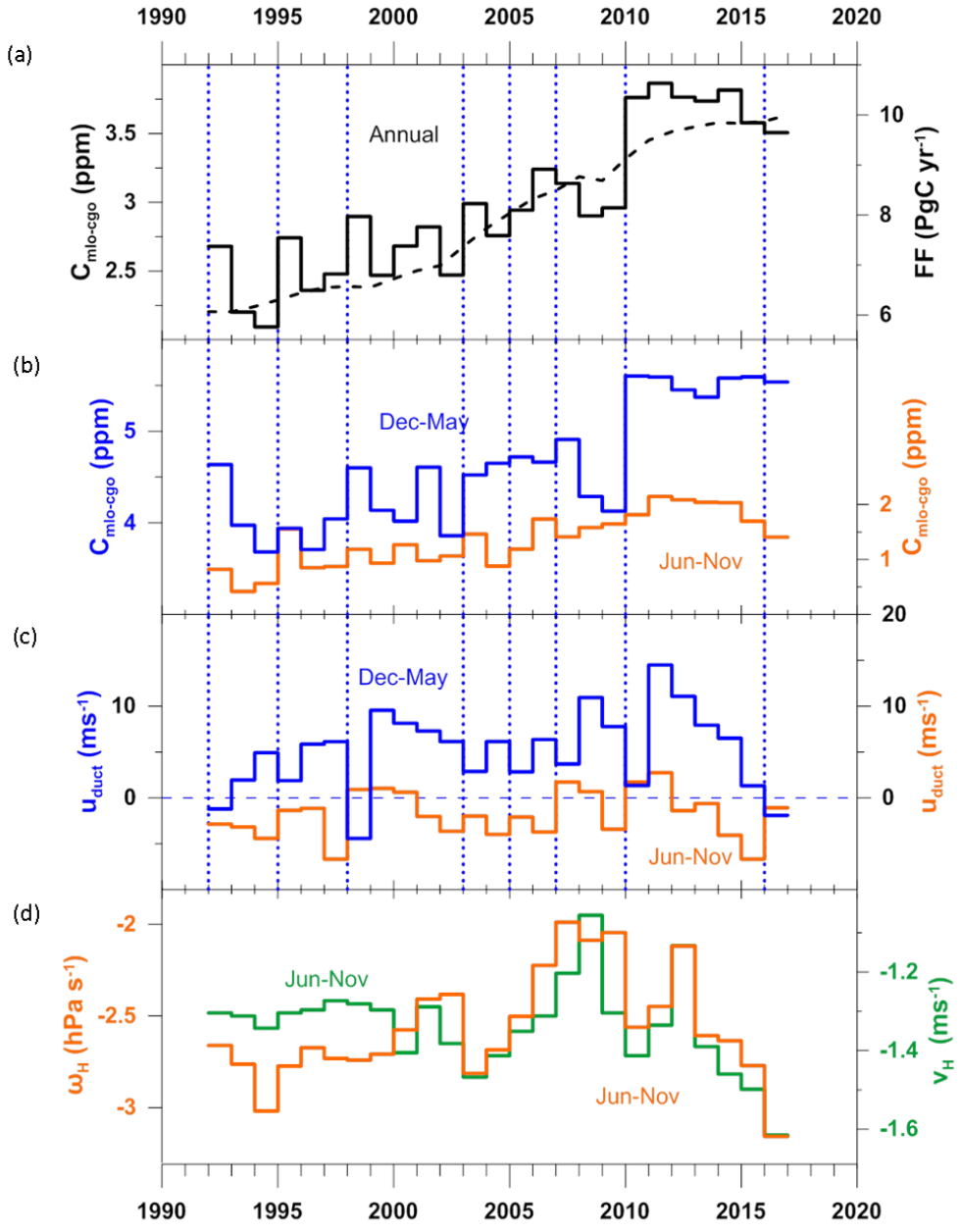

Figure 2: (a) Annual average $C_{mlo-cgo}$ (solid) and global CO_2 emission estimate (dashed) for 1992 to 2016, (b) $C_{mlo-cgo}$ for boreal winter-spring (blue) and summer-autumn (orange), (c) u_{duct} for boreal winter-spring (blue) and summer-autumn (orange), (d) boreal summer-autumn ω_H (orange) and v_H (green).

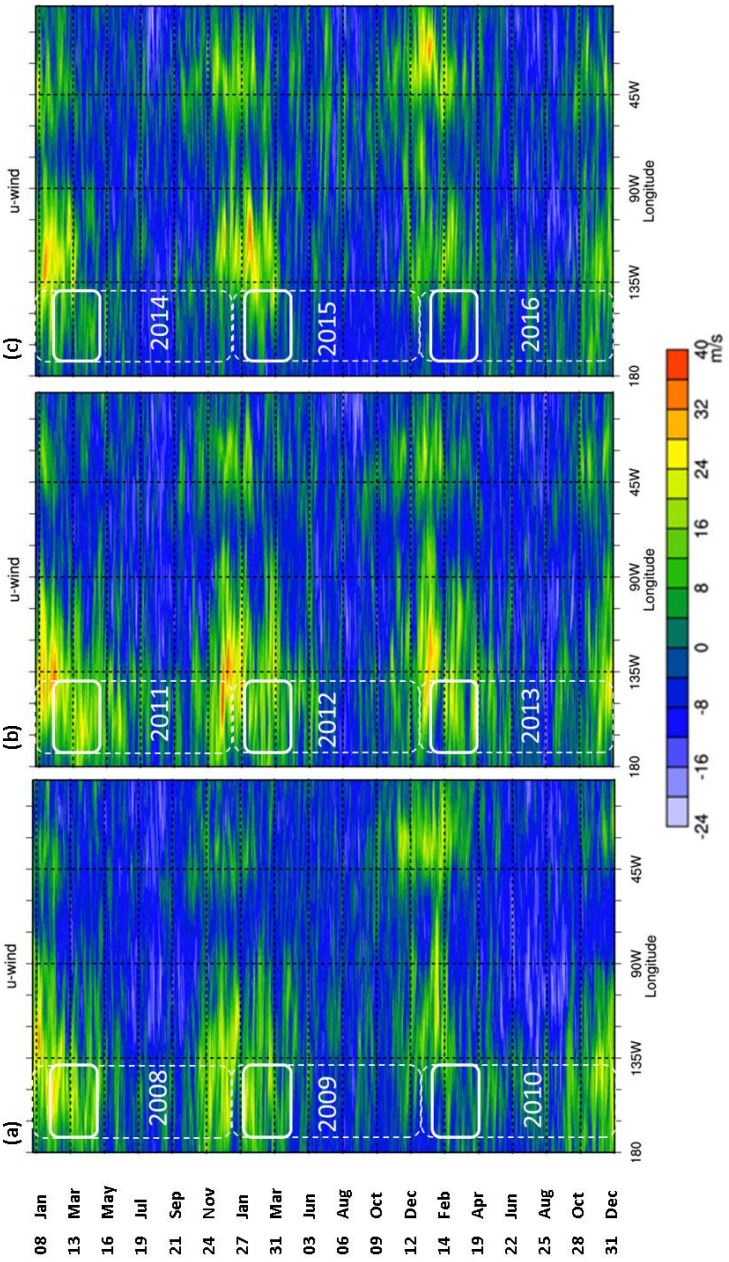

Figure 3: Hovmoller diagrams of 300 hPa zonal wind (ms^{-1}) averaged between 5S and 5N as a function of longitude and time for (a) 1 January 2008 to 31 December 2010, (b) 1 January 2011 to 31 December 2013 and (c) 1 January 2014 to 31 December 2016. Green through to red represent westerly winds (u -winds, ms^{-1}) over the Western Hemisphere. White solid rounded rectangles denote the longitudinal extent of the Pacific duct and the height denotes the February to April period.

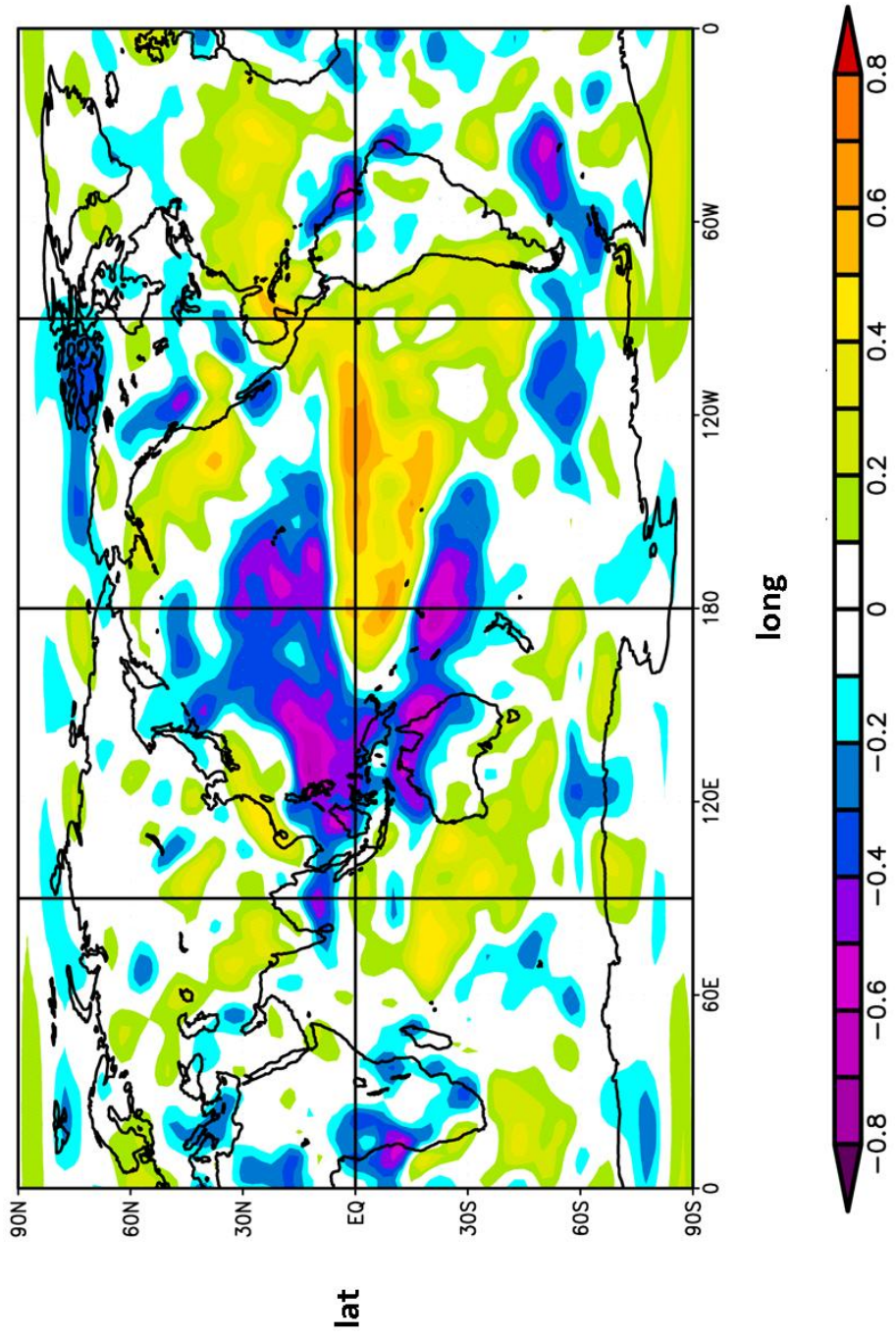

Figure 4: Correlation of vertical velocity ω (Pas^{-1}) at 300 hPa with SOI for Feb-Apr and 1948-2016.

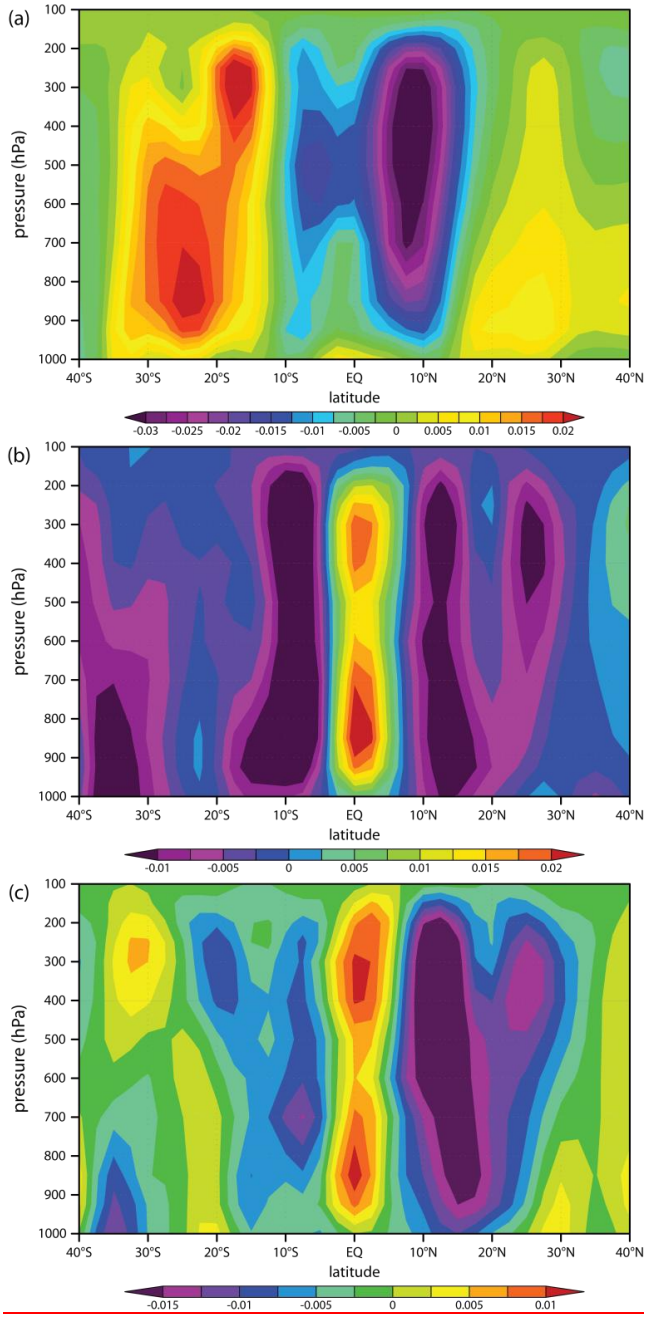

Figure 5: Latitude height cross section of June to August 120E-240E average (a) ω (Pas^{-1}) – vertical velocity in pressure coordinates – for 1979-2016, (b) ω difference of 2016 minus 1979-2016, (c) ω difference of 2016 minus 2010.

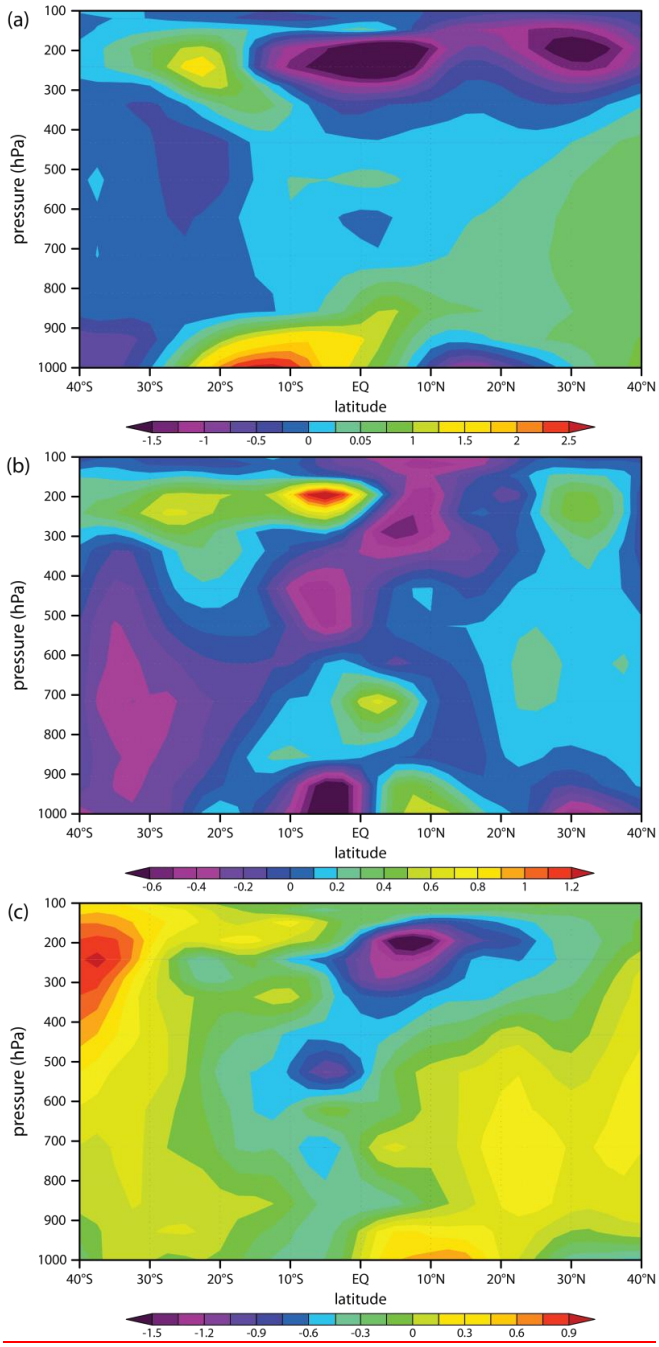

Figure 6: Latitude height cross section of June to August 120E-240E average (d) meridional wind v (ms^{-1}) for 1979-2016, (e) meridional wind v difference of 2016 minus 1979-2016 and (f) meridional wind v difference of 2016 minus 2010.

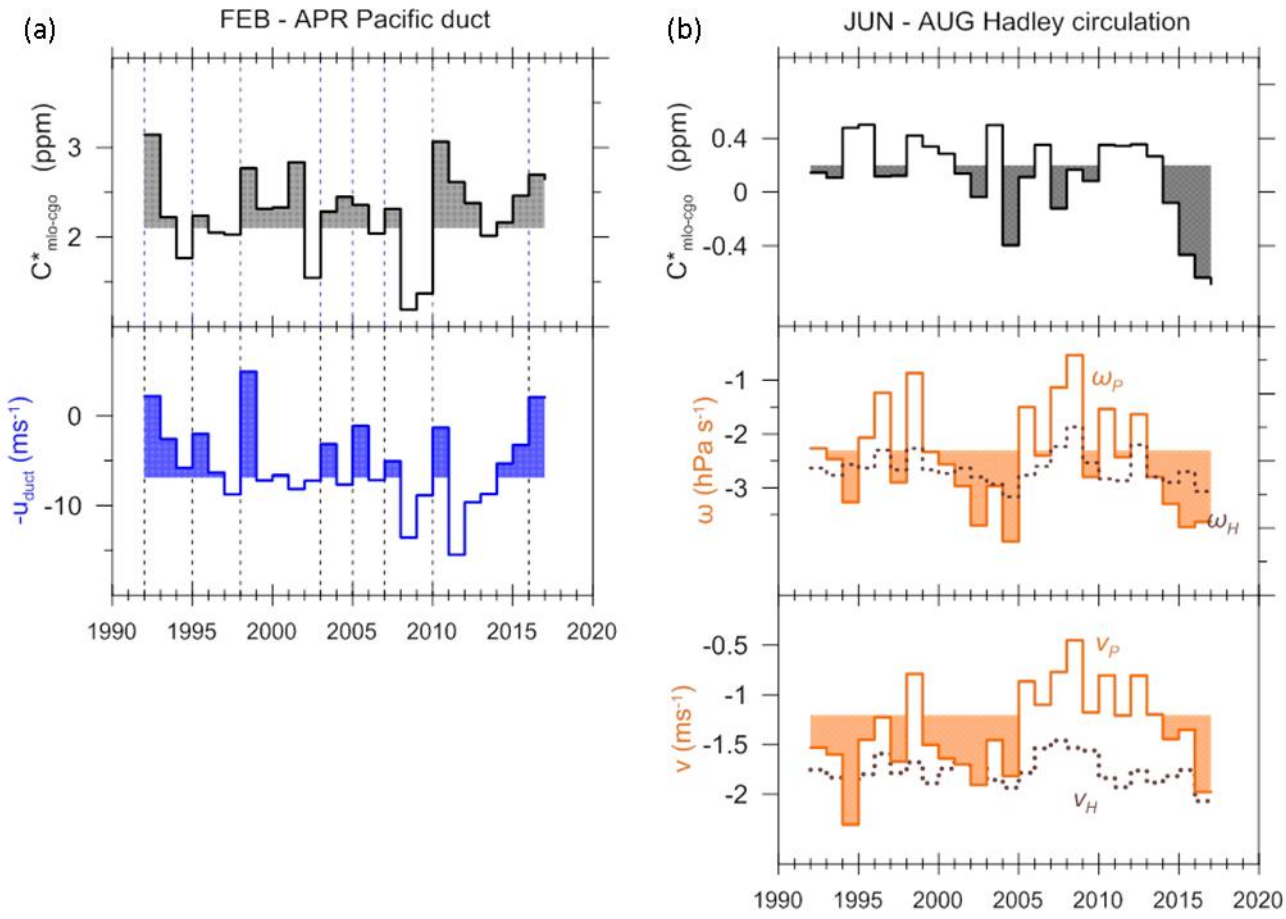

Figure 7: (a) $C^*_{mlo\text{-}cgo}$ and $-u_{duct}$ averaged between Feb-Apr for 1992-2016 and (b) $C^*_{mlo\text{-}cgo}$, ω_P, ω_H, v_P and v_H averaged between Jun-Aug for 1992-2016 .

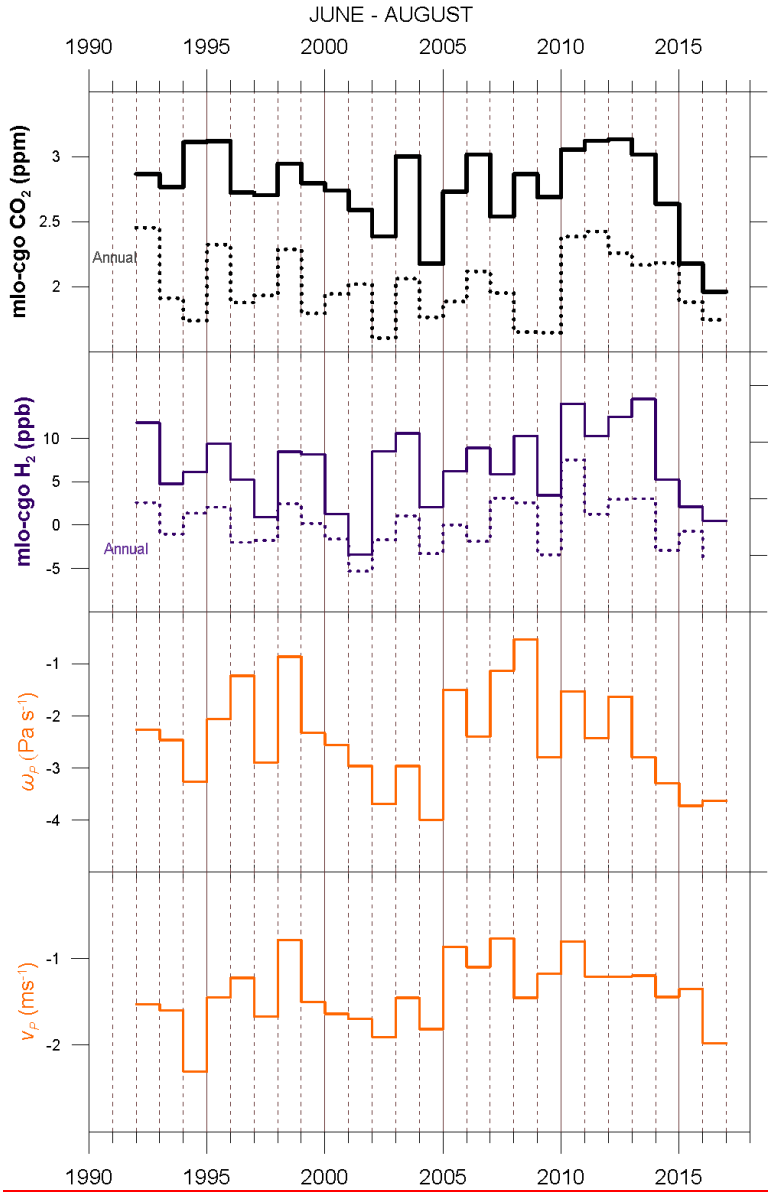

Figure 8: Time series of June–August and Annual averages of detrended mlo–cgo differences in CO_2 and H_2 and June–August average dynamical indices ω_P and v_P .

Supplement of

Unprecedented strength of Hadley circulation in 2015-2016 impacts on CO_2 interhemispheric difference

Jorgen S. Frederiksen and Roger J. Francey

CSIRO Oceans and Atmosphere, Aspendale, Victoria, AUSTRALIA

Correspondence to: Jorgen S. Frederiksen (jorgen.frederiksen@csiro.au)

SUPPLEMENTARY INFORMATION

1 Pacific and Atlantic westerly ducts

The interhemispheric response to mid-latitude forcing produced by Rossby dispersion through equatorial westerly ducts was documented by Webster and Holton (1982). The zonal winds in the equatorial troposphere are generally easterly but in the upper troposphere the winds may be westerly in the Pacfic duct (centred on 5°N-5°S, 140°W-170°W) or the Atlantic duct (centred on 5°N-5°S, 10°W-40°W) as shown in Figure 2 of Webster and Chang (1988). As discussed in Francey and Frederiksen (2016, denoted FF16), and shown in Figure 1S for the period 1992 to 2016 of interest here, the upper-tropospheric zonal wind is strongly correlated with the SOI in the Pacific duct region and anti-correlated in the Atlantic duct region. As the atmospheric circulation changes between La Niña and El Niño conditions the warm ocean temperatures move from the western to eastern Pacific. The upward branch of the Walker circulation follows the warm water and the associated upper-tropospheric westerlies to the east of the uplift successively open the Pacific westerly duct and then the Atlantic westerly duct (Figure 1 of Webster and Chang 1988). This is the reason for the correlations in our Figure 1S. The strength (and sign) of the upper-tropospheric zonal velocity in the near-equatorial regions is correlated with corresponding levels in the turbulent kinetic energy which is generated by Rossby wave breaking (Figure 6 of Frederiksen and Webster 1988). The Pacific duct, u_{duct} of Table 1, is in general the dominant duct as shown in Figure 2S which depicts the boreal winter (Dec-Feb) upper tropospheric vector wind for 1992-2016.

2~~1~~ Topographic Rossby waves during February 2015

As noted in the Introduction, the NASA (2016) OCO-2 CO_2 concentration in Figure 1~~b~~(a) shows Rossby wave trains over the eastern Pacific and across South America on 17 February 2015. This episode is characteristic of other times of IH Rossby wave propagation during the boreal winter–spring, and particularly February, of 2015. The average 17 to 18 February 2015 streamfunction anomaly, from the thirty year 1981–2010 mean for the same period, is shown in Figure ~~1~~3S(a) for the

Western Hemisphere (0°W–180°W) between 60°S and 60°N and at the $\sigma = 0.2582$ level. Here $\sigma = \frac{pressure}{surface\ pressure}$ and the corresponding pressure level is circa 260 hPa. We note that the phase lines broadly run from SW to NE between the Southern and Northern Hemispheres but are modulated by some smaller scale features. Moreover the dominant zonal wavenumber $m = 4$.

Indeed there are broad similarities between the streamfunction anomaly in Figure ~~1~~3S(a) and the streamfunction for the purely topographic Rossby waves in Figures 3a and b of Frederiksen and O'Kane (2005). For both the observations considered here and the ensemble of nonlinear simulations and statistical closure calculations the phase lines in the Western Hemisphere run SW to NE and the dominant wavenumber is 4. The dominant wavenumber 4 is also clearly seen in the energy spectra in Figure 2 of Frederiksen and O'Kane (2005). The SW to NW phase lines of pure topographic Rossby waves are also seen in the linear calculations in Figure 6 of Frederiksen (1982). In both the linear and nonlinear calculations the topographic Rossby waves are generated by the interaction of westerly winds with a conical mountain located at 30° N (an idealized representation of the massive Himalayan orography) and for a situation where the near equatorial winds are westerly. For the observational results in Figure ~~1~~3S(a), the near equatorial winds between 5°S and 5°N are westerly in the Western Hemisphere broadly above 400 hPa and easterly below (not shown).

Figure ~~1~~3S(b) shows the 300 hPa zonal wind anomaly corresponding to the average 17 to 18 February streamfunction anomaly in Figure ~~1~~3S(a). Again the SW to NE phase lines are evident as is the dominant $m = 4$ wavenumber although the presence of smaller scale features associated with disturbances in the storm tracks (typically $m \sim 8-12$) is perhaps more evident. In Figures ~~2~~4S(a) and ~~2~~4S(b) we depict latitude pressure cross sections of the zonal wind anomalies for 17 to 18 February averaged between 120°W–140°W and 80°W–100°W respectively. We note that the anomaly is largely equivalent barotropic, as expected for topographic Rossby waves, and, by comparing the two panels, the SW to NW phase tilt is evident throughout the atmosphere. It can also be seen that the propagation across the equator into the Southern Hemisphere occurs primarily in the upper troposphere, particularly between 80°W–100°W where the mean westerly winds are weaker (not shown).

We have also plotted latitude pressure cross sections of anomalies of the vertical velocity in pressure coordinates, $\omega = dp/dt$ where p is pressure, for 17 to 18 February averaged between 120°W–140°W and 80°W–100°W (not shown). These cross sections indicate that there is strong uplift in the Northern Hemisphere between 10°N and 30°N (negative ω) and general descent south of that band to 30°S. The topographic Rossby wave train generated by westerly winds impinging on the Himalayas may interact with a small region of uplift focused over the Andes in Peru (not shown) when it crosses into the Southern Hemisphere. However, in addition it should be noted that the wave train occurs at a time of seasonal minimum in Southern Hemisphere CO_2.

~~2 Interhemispheric exchange of trace gases~~

Next, we consider the eddy and mean IH exchange of other trace gas species and their correlations with CO_2 and dynamical indices of transport. We focus on Feb-Apr for eddy transport and Jun-Aug for mean transport since these periods were the peaks for correlations of CO_2 IH difference with eddy and mean transport indices respectively. However, there are differences in the seasonal variability in the different trace gas species that are reflected in their transport and for that reason we also briefly mention the results for other time periods. We begin by further examining Mauna Loa minus Cape Grim (mlo-cgo) differences, between 1992-2016, in the routinely monitored CSIRO species CH_4, CO and H_2 in addition to CO_2 that were briefly considered in Frederiksen and Francey (FF16), as well as N_2O (for 1993-2016). Thereafter we discuss mlo-cgo differences in SF_6 data sourced from the NOAA Halocarbons and other Atmospheric Trace Species Group (HATS) program from 1998 (NOAA, 2018).

2.1 Pacific westerly duct and eddy IH transport of CSIRO monitored trace gases

The IH exchange of the trace gas species CH_4, CO and H_2, in addition to CO_2, and the role of the Pacific westerly wind duct was also considered in FF16. In particular, the covariance, of the mlo-cgo difference in these routinely monitored CSIRO species with u_{duct}, is shown in Figure 5 of FF16. We recall that the u_{duct} index is the average zonal wind in the region 5°N to 5°S, 140°W to 170°W at 300hPa. As noted in FF16, the extreme cases of Pacific westerly duct closure in 1997-98 and 2009-10 show up in the absence of seasonal IH exchange for CH_4 and CO as well as CO_2. The similar behaviour of detrended anomalies of mlo-cgo difference in CH_4, CO and CO_2 and their correlations with u_{duct} is shown in Table 1S for Feb-Apr. We note the quite high correlations of CH_4 and CO with CO_2 ($r = 0.697$ and $r = 0.645$ respectively) and the significant anti-correlations of all these three species with u_{duct} ($r = -0.448$, $r = -0.605$ and $r = -0.500$ respectively). In fact, for Mar-May the correlation between CH_4 and CO_2 is even larger at $r = 0.728$ (and with u_{duct} it is $r = -0.474$) while between CO and CO_2 it is $r = 0.611$ (and with u_{duct} it is $r = -0.507$). These results are of course consistent with Figure 5 of FF16 and are further evidence of similarities of IH transient eddy transport of these three gases. Table 1S also shows that the Feb-Apr correlation of H_2 with CO_2 and anti-correlation with u_{duct} have smaller magnitudes ($r = 0.296$ and $r = -0.218$ respectively) although the Nov-Apr anti correlation of H_2 with u_{duct} is more comparable with $r = -0.463$. These results for anomalies are probably related to corresponding similarities and differences in the seasonal mean values (not shown) of these gases in Feb-Apr, as discussed below.

Anomalies in mlo-cgo differences in CSIRO monitored N_2O are generally poorly correlated with those in CO_2 as shown for Feb-Apr and Jun-Aug in Tables 1S and 2S respectively (the maximum 3-month average correlation is $r = 0.274$ for Mar-May) and this is reflected in generally poor correlation with the dynamical indices shown in Tables 1S and 2S. This reflects the fact that natural exchanges with equatorial agriculture and oceans are the main sources (Ishijima et al., 2009), and the seasonal range in mlo-cgo difference is only around 0.2% of the mean N_2O level, more than 10 times less than is the case for the other species.

2.2 Hadley circulation and mean IH transport of CSIRO monitored trace gases

We examine the role of the Hadley circulation on the mean transport of trace gases focusing on the boreal summer period of Jun–Aug. Table 2S shows the correlations between the detrended anomalies of mlo–cgo difference in CH_4, CO and H_2 with CO_2 and with the dynamical indices ω_p and v_p. Recall that ω_p is the 300 hPa vertical velocity in pressure coordinates, between 10°N–15°N, and v_p is the 200 hPa meridional wind, between 5°N–10°N, and both are averaged over the 120°E–240°E Pacific sector. We note that the largest Jun–Aug correlation is between H_2 and CO_2 ($r = 0.680$) and the correlations between CH_4 and CO with CO_2 are considerably smaller ($r = 0.246$ and $r = 0.108$ respectively) while for Apr–Jun the latter correlations are more comparable at $r = 0.583$ and $r = 0.496$ respectively.

These correlations with CO_2 are also reflected in the respective correlations of the other trace gases with ω_p and v_p. We note from Table 2S that the Jun–Aug correlations of H_2 with ω_p and v_p are $r = 0.427$ and $r = 0.442$ respectively which is slightly less than the corresponding correlations between CO_2 and the dynamical indices ($r = 0.522$ and $r = 0.539$ respectively) but considerably larger than for CH_4 and CO. For May–Jul the correlation of H_2 with ω_p is slightly larger with $r = 0.526$.

Again, the different behaviour of the trace gas anomalies may be related to their different seasonal mean values; the seasonal mean IH difference for H_2 peaks in boreal summer while for CH_4 and CO it is relatively low with a minimum in August. The distribution and variability of surface exchange is different for each of the trace gases and there is potential for this to interact with the restricted extent and seasonal meandering of the regions of uplift to influence IH exchange of a species. For example, 70% of the global total CH_4 emissions are from mainly equatorial biogenic sources that include wetlands, rice agriculture, livestock, landfills, forests, oceans and termites (Denman et al., 2007) and CO emissions contain a significant contribution from CH_4 oxidation and from tropical biomass burning.

A more detailed examination of the inter–annual variation of the mlo–cgo difference in H_2 during boreal summer is presented in Figure 3S. It shows the detrended H_2 data in comparison with the corresponding CO_2 data and with the ω_p and v_p indices. First we note that the detrended CO_2 data in the top panel has very similar inter–annual variation to the FF–adjusted $C^*_{mlo-cgo}$ in Figure 6b. We also see that the qualitative behaviour of H_2 mirrors many aspects of CO_2, as expected from the correlations in Table 2S. In particular, the increase in the IH difference of H_2 in 2010 is even more pronounced than for CO_2. For CO_2 and for H_2 there is a steady reduction in the IH difference from around 2013 leading to a local minimum in 2016. In both of these respects these gases broadly follow the changes in the Hadley circulation including the strengthening during 2015–2016. Vertical lines in Figure 3S indicate other times between 1992 and 2016 when transitions occur in both these trace gases and in the Hadley circulation characterized by ω_p and v_p.

Surface exchanges of H_2 have similarities to those of CO_2 in that they occur mostly at mid–northern latitudes and are mainly due to emissions from Fossil Fuel combustion. However H_2 also has mid–northern latitude photochemical sources peaking in August (Price et al., 2007). These boreal summer sources are almost offset by a combined soil and hydroxyl sink, but the overall interhemispheric partial pressure difference is boosted by a significant reduction in the Southern Hemisphere

photochemical source at that time. For both species, the most northern excursions of the inter-tropical convergence zone that occurs at Pacific latitudes encounter increasing concentrations of both gases.

As noted above, anomalies in mlo-cgo differences in N_2O are poorly correlated with those in CO_2 and in dynamical indices (Tables 1S and 2S). Indeed the 3-month average anti-correlation with u_{auct} that has the largest magnitude is $r = -0.133$ for Mar-May and the largest correlations with ω_p is $r = 0.359$ for Apr-Jun and with v_p is $r = 0.350$ for May-Jul.

2.3 Interhemispheric exchange of SF_6

In the case of SF6 we have analysed the mlo-cgo difference in available NOAA HATS data from 1998 to 2012 when cgo HATS measurements ceased. Correlations of detrended anomalies in IH differences in SF_6 with those in CO_2 are as follows: the Feb-Apr correlation is $r = 0.619$, the Mar-May correlation is $= 0.722$, the Apr-Jun correlation is $r = 0.595$, the May-Jul correlation is $r = 0.303$ and the Jun-Aug correlation is $r = 0.223$. The corresponding correlations with dynamical indices are as follows: for Feb-Apr the correlation with u_{auct} is $r = -0.617$, the May-Jul correlations with ω_p is $r = 0.465$, the Jun-Aug correlation with ω_p is $r = 0.433$, the May-Jul correlation with v_p is $r = 0.517$ and the Jun-Aug correlation with v_p is $r = 0.385$. We note that SF_6 has an anti-correlation with u_{auct} for Feb-Apr that has larger magnitude than for CO_2 and even CH_4. Thus, there is again a significant influence of the Pacific westerly duct, in late boreal winter and spring, and of the Hadley circulation, in boreal summer and late spring, as measured by these indices, on the mlo-cgo differences of SF_6; these SF_6 differences exhibit a similar step change in 2009-2010 as shown for CO_2 in Figures 2 and 6.

2.4 Implications for constaining terrestrial biosphere exchange

The sign and strength of zonal winds in the Pacific westerly duct (u_{auct}) are correlated with corresponding changes in near-equatorial transient kinetic energy (Fig. 6, Frederiksen and Webster 1988) resulting in changes in the mixing of trace gases. This effect may not be adequately represented in the parameterizations used in atmospheric transport models. Model determinations of short term variations in the Hadley circulation exchange are also susceptible to uncertainties in representations of the equatorial convective dynamics (Lintner et al. 2004). By identifying spatial changes due to transport and providing empirical indices that describe short-term variations in both Pacific westerly duct and Hadley transfers there is potential to improve atmospheric constraints on Dynamic Vegetation modelling.

Acknowledgements. We thank Nada Derek and Stacey Osbrough for assistance with the graphics. The dynamics contributions were prepared using data and software from the NOAA/ESRL Physical Sciences Division web site: http://www.esrl.noaa.gov/psd/. The trace gas data for CSIRO monitored species CO_2, CH_4, CO, H_2 and N_2O and the NOAA monitored SF_6 are available from the World Data Centre for Greenhouse Gases website: https://ds.data.jma.go.jp/gmd/wdcgg/cgi-bin/wdcgg/catalogue.cgi

References

1. Denman, K. L., Brasseur, G., Chidthaisong, A., Ciais, P., Cox, P. M., Dickinson, R. E., Hauglustaine, D., Heinze, C., Holland, E., Jacob, D., Lohmann, U., Ramachandran, S., da Silva Dias, P. L., Wofsy, S. C., & Zhang, X.: Couplings Between Changes in the Climate System and Biogeochemistry. In: *Climate Change 2007: The Physical Science Basis. Contribution of Working Group I to the Fourth Assessment Report of the Intergovernmental Panel on Climate Change* [Solomon, S., Qin, D., Manning, M., Chen, Z., Marquis, M., Averyt, K.B., Tignor, M. & Miller, H.L. (eds.)]. Cambridge University Press, Cambridge, United Kingdom and New York, NY, USA, 2007.

2.1. Francey, R. J., & Frederiksen, J. S.: The 2009–2010 step in atmospheric CO_2 interhemispheric difference, Biogeosciences, 13, 873–885, doi: 10.5194/bg-13-873-2016, 2016.

3.2. Frederiksen, J. S.: Eastward and westward flows over topography in nonlinear and linear barotropic models, J. Atmos. Sci., 39, 2477–2489, 1982.

4.3. Frederiksen, J. S., & O'Kane, T. J.: Inhomogeneous closure and statistical mechanics for Rossby wave turbulence over topography, J. Fluid Mech., 539, 137–165, 2005.

4. Frederiksen, J. S., & Webster, P. J.: Alternative theories of atmospheric teleconnections and low-frequency fluctuations, Rev. Geophys., 26, 459–494, 1988.

5. Webster, P. J., & Chang, H. R.: Equatorial energy accumulation and emanation regions: Impacts of a zonally varying basic state, J. Atmos. Sci., 45, 803-829, 1988.

5.6. Webster, P. J., & Chang, H. R.: Equatorial energy accumulation and emanation regions: Impacts of a zonally varying basic state, J. Atmos. Sci., 45, 803-829, 1988.

6. Ishijima, K., Nakazawa, T., & Aoki, S.: Variations of atmospheric nitrous oxide concentration in the northern and western Pacific, Tellus B, 61:2, 408–415, doi: 10.1111/j.1600-0889.2008.00406.x, 2009.

7. Lintner, B. R., Gilliland, A. B., & Fung, I. Y.: Mechanisms of convection-induced modulation of passive tracer interhemispheric transport interannual variability, J. Geophys. Res., 109, D13102, doi:10.1029/2003JD004306, 2004.

8.7. NASA: Following carbon dioxide through the atmosphere, 2016. - https://svs.gsfc.nasa.gov/12445 https://www.nasa.gov/feature/goddard/2016/eye-popping-view-of-co2-critical-step-for-carbon-cycle-science

9. Price, H., Jaeglé, L., Rice, A., Quay, P., Novelli, P. C., & Gammon, R.: Global budget of molecular hydrogen and its deuterium content: Constraints from ground station, cruise, and aircraft observations, J. Geophys. Res., 112, D22108, doi:10.1029/2006JD008152, 2007.

10. NOAA, 2018. http://www.esrl.noaa.gov/gmd/

Tables

Table 1S: Correlations (r) between the detrended mlo–cgo gas anomalies for CO_2, CH_4, CO and H_2 with CO_2 and u_{40E} index of transient transport averaged between Feb–Apr for 1992–2016. Also shown are corresponding correlations for N_2O and 1993–2016 and for SF_6 and 1998–2012.

Gas	CO_2	u_{duct}
CO_2	$r = 1.0$	$r = -0.500$
CH_4	$r = 0.697$	$r = -0.448$
CO	$r = 0.645$	$r = -0.605$
H_2	$r = 0.296$	$r = -0.218$
N_2O	$r = 0.215$	$r = -0.088$
SF_6	$r = 0.619$	$r = -0.617$

Table 2S: Correlations (r) between the detrended mlo–cgo gas anomalies for CO_2, CH_4, CO and H_2 with CO_2 and indices of mean transport, ω_p and v_p averaged between Jun–Aug for 1992–2016. Also shown are corresponding correlations for N_2O and 1993–2016 and for SF_6 and 1998–2012.

Gas	CO_2	ω_p	v_p
CO_2	$r = 1.0$	$r = 0.520$	$r = 0.534$
CH_4	$r = 0.246$	$r = 0.195$	$r = 0.250$
CO	$r = 0.108$	$r = 0.205$	$r = 0.236$
H_2	$r = 0.680$	$r = 0.427$	$r = 0.442$
N_2O	$r = -0.010$	$r = 0.290$	$r = 0.266$
SF_6	$r = 0.223$	$r = 0.433$	$r = 0.385$

Figures

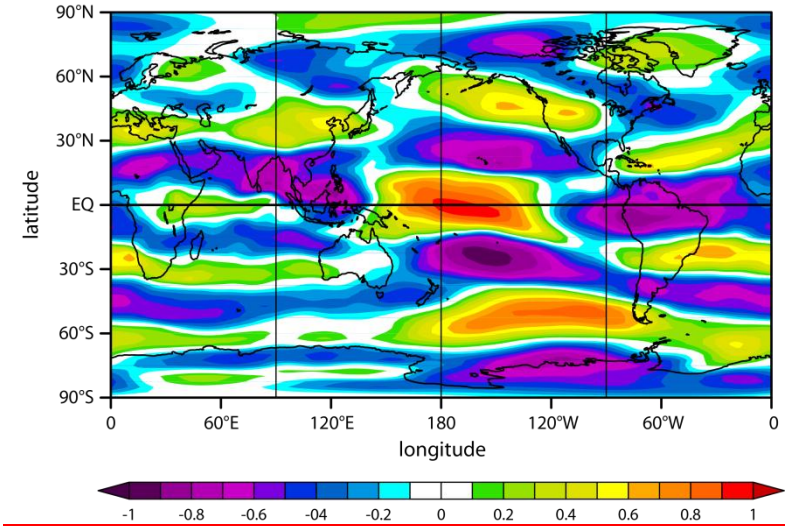

Figure 1S: Correlation over the annual cycle of 1992-2016 upper-tropospheric winds (300 hPa) with the Southern Oscillation Index (SOI).

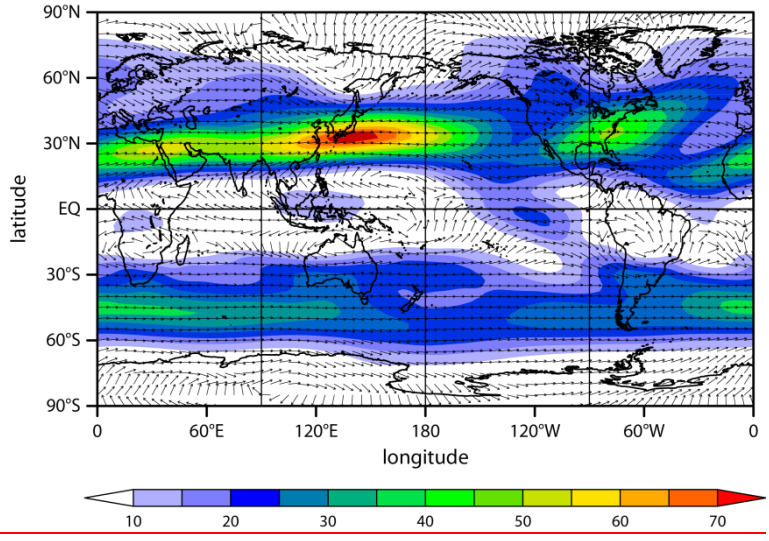

Figure 2S: Upper-tropospheric (200 hPa) boreal winter (Dec-Feb) vector wind (ms^{-1}) for 1992-2016.

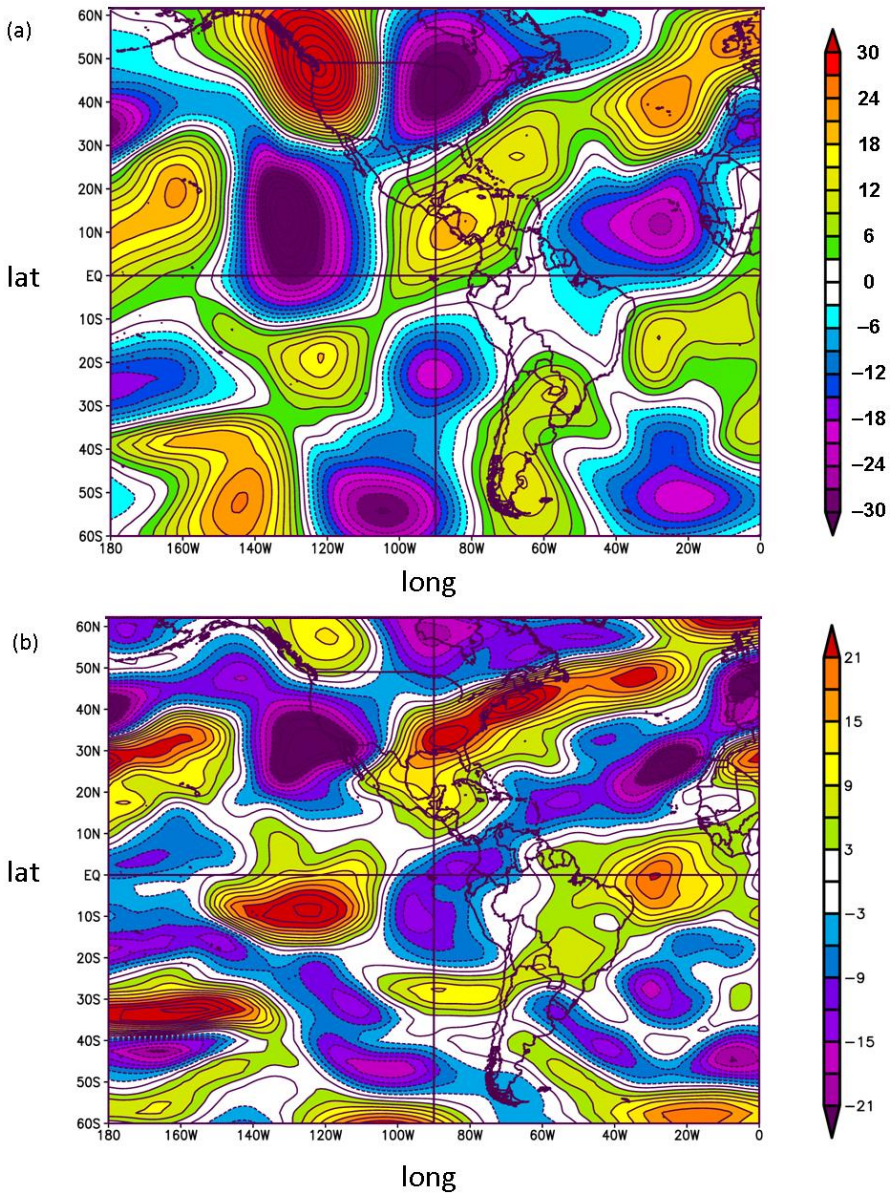

Figure 3S: The average 17 to 18 February 2015 (a) streamfunction anomaly at $\sigma = 0.2582$ in kms^{-1} and (b) zonal wind anomaly at 300 hPa in ms^{-1} where the anomalies are with respect to the thirty year 1981–2010 mean for the same period.

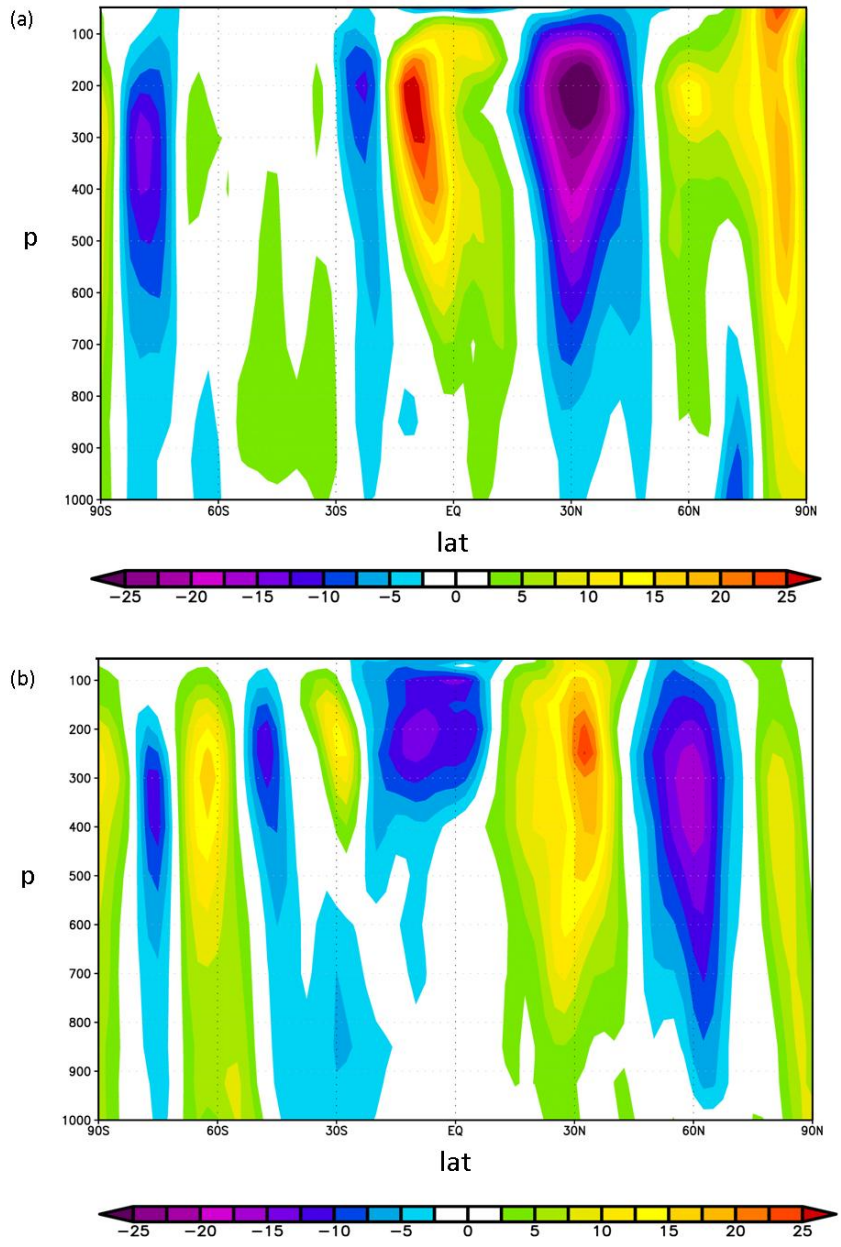

Figure 4S: Latitude pressure (hPa) cross sections of zonal wind anomalies in ms^{-1} for 17 to 18 February 2015 averaged between (a) 120°W–140°W and (b) 80°W–100°W.

~~**Figures**~~

~~Figure 1S~~

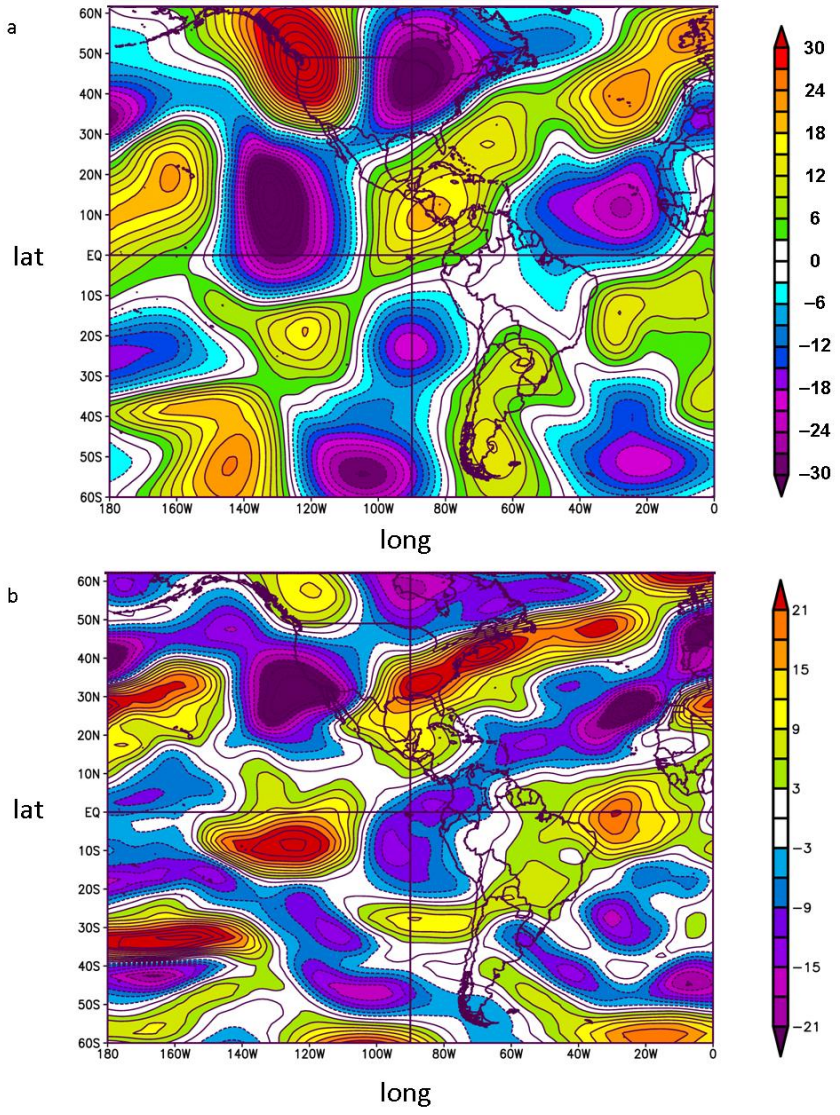

~~Figure 1S: The average 17 to 18 February 2015 (a) streamfunction anomaly at $\sigma = 0.2582$ in kms^{-1} and (b) zonal wind anomaly at 300 hPa in ms^{-1} where the anomalies are with respect to the thirty year 1981–2010 mean for the same period.~~

~~Figure 2S~~

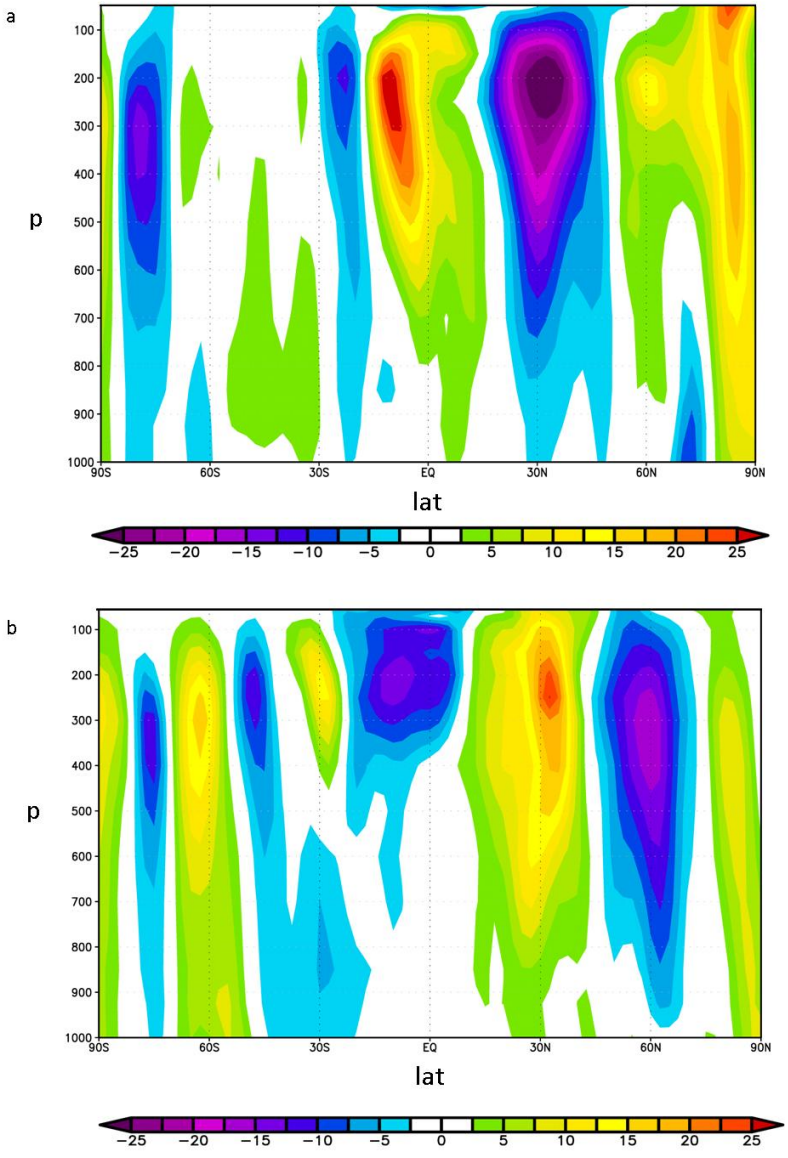

~~Figure 2S: Latitude pressure cross sections of zonal wind anomalies in ms^{-1} for 17 to 18 February 2015 averaged between (a) 120°W–140°W and (b) 80°W–100°W.~~

~~Figure 3S~~

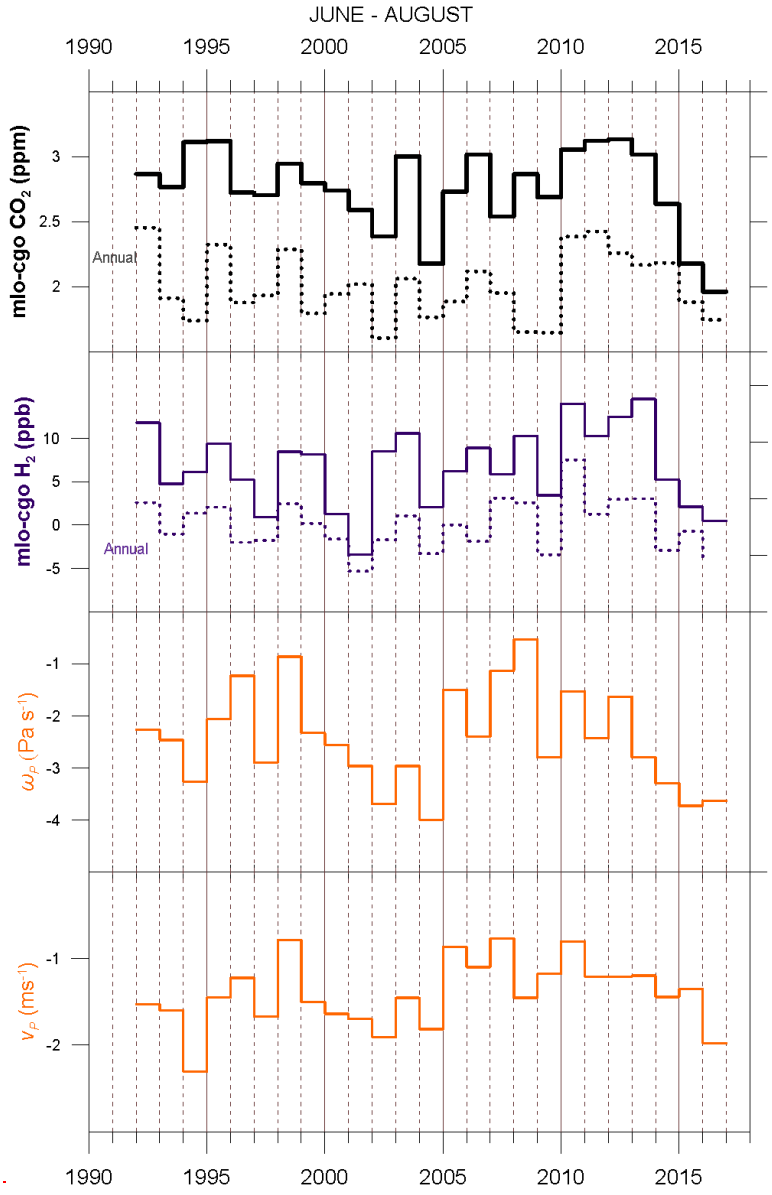

~~Figure 3S: Time series of June–August and Annual averages of detrended mlo–cgo differences in CO_2 and H_2 and June–August average dynamical indices ω_p and v_p.~~